

UAV-BASED POTHOLE IDENTIFICATION: A PHOTOGRAMMETRIC  
APPROACH

by

Jin Kyu Lee  
A Thesis  
Submitted to the  
Graduate Faculty  
of  
George Mason University  
in Partial Fulfillment of  
The Requirements for the Degree  
of  
Master of Science  
Geoinformatics and Geospatial Intelligence

Committee:

_____	Dr. Sven Fuhrmann, Thesis Director, Associate Professor
_____	Dr. Arie Croitoru, Committee Member, Associate Professor
_____	Dr. Matthew Rice, Committee Member, Associate Professor
_____	Dr. Dieter Pfoser, Committee Member, Professor
_____	Dr. Dieter Pfoser, Department Chair
_____	Dr. Donna M. Fox, Associate Dean, Office of Student Affairs & Special Programs, College of Science
_____	Dr. Peggy Agouris, Dean, College of Science
Date: _____	Spring Semester 2019 George Mason University Fairfax, VA

UAV-based Pothole Identification: A Photogrammetric Approach

A Thesis submitted in partial fulfillment of the requirements for the degree of Master of Science at George Mason University

by

Jin Kyu Lee  
Bachelor of Science  
George Mason University, VA 2016

Director: Sven Fuhrmann, Associate Professor  
George Mason University

Spring Semester 2019  
George Mason University  
Fairfax, VA

Copyright 2019 Jin Kyu Lee  
All Rights Reserved

## **DEDICATION**

This is dedicated to my family and friends who have supported me continuously as I struggled and plugged away at this project.

## **ACKNOWLEDGEMENTS**

I would like to thank my family, close friends, relatives, and supporters who have made this happen. I would also like to thank Dr. Sven Fuhrmann, Dr. Matthew Rice, Dr. Arie Croitoru, Dr. Dieter Pfoser, and Dr. Kevin Curtin for helping me throughout my research and graduate career. I have learned so much from them during my graduate career, and without them, I would not be where I am. Also, I would like to thank the GGS department staff: Sam Cooke, Emmy Daniels, and Steve Humiston for being supportive and helpful with everything behind the scene. Thank you everyone for encouraging and supporting me to complete this research.

## TABLE OF CONTENTS

	Page
List of Tables .....	vii
List of Figures .....	viii
List of Abbreviations .....	x
Abstract .....	xi
Chapter One: Introduction .....	1
1.1 Introduction .....	1
1.2 Thesis Objectives .....	6
1.3 Thesis Organization.....	8
Chapter Two: Background and Literature Review .....	9
2.1 Pavement Condition Assessment .....	9
2.2 Existing Pothole Detection Methods.....	11
Vibration-based .....	11
2D Vision-based .....	13
3D Reconstruction-based.....	15
2.3 Unmanned Aerial Vehicle Systems.....	16
UAV Overview .....	17
UAV Remote Sensing .....	19
UAV Photogrammetry.....	20
Chapter Three: Data and Method.....	23
3.1 Overview .....	23
3.2 Equipment and Tools .....	25
3.3 Pilot Study .....	31
3.4 Data Processing.....	38
3.5 GIS Development.....	41
3.6 3D Reconstruction.....	45
3.7 Image Processing Detection.....	54

Chapter Four: Results .....	57
4.1 Pilot Study 1 .....	57
4.2 Pilot Study 2 .....	70
Chapter Five: Conclusions .....	82
5.1 Future Research.....	83
References .....	84

## LIST OF TABLES

Table	Page
Table 1. Common Pothole Severity Levels .....	4
Table 2. Common UAS for Remote Sensing.....	18
Table 3. Detailed Mavic 2 Pro Specifications .....	26
Table 4. Pilot Study 1 Ground Truth Measurement.....	59
Table 5. Pilot Study 1 Identified Measurement .....	70
Table 6. Pilot Study 1 Identified Measurement Accuracy .....	70
Table 7. Pilot Study 2 Ground Truth Measurement.....	72
Table 8. Pilot Study 2 Identified Measurement .....	80
Table 9. Pilot Study 2 Identified Measurement Accuracy.....	80

## LIST OF FIGURES

Figure	Page
Figure 1. Structure of Concrete and Asphalt Pavement , American Concrete Pavement Association.....	2
Figure 2. Different Stages of Pothole Development and Formation .....	3
Figure 3. UAV Captured Image.....	6
Figure 4. Manually Identified Pothole.....	7
Figure 5. Pavement Condition Assessment Platform .....	10
Figure 6. Vibration-based System Schematics .....	12
Figure 7. Acceleration Records.....	13
Figure 8. 2D-based Detection Method Workflow .....	14
Figure 9. 3D-based Collection Measurement System.....	16
Figure 10. Consumer-grade UAVs: Left to Right (a) – (e).....	19
Figure 11. Mavic 2 Pro Aircraft Diagram.....	25
Figure 12. Pix4Dmapper and Pix4capture Screen .....	28
Figure 13. ArcMap 10.6.1 with Main Data.....	29
Figure 14. CloudCompare Graphical User Interface .....	30
Figure 15. Pilot Study Test Sites.....	32
Figure 16. Pilot Study Process .....	33
Figure 17. Example of Ground Truth Measurement Tools.....	36
Figure 18. Pothole Samples with Ground Truth Data.....	37
Figure 19. Pix4D Processing Options.....	38
Figure 20. Orthomosaic of Test Site Before and After Clip.....	41
Figure 21. Roadways and Centerlines Data.....	42
Figure 22. Example of Pothole Shapefile Data.....	44
Figure 23. Importing, Segmenting and Clipping Point Cloud.....	47
Figure 24. Before and After Noise Removal of Point Cloud Data .....	48
Figure 25. 2.5D Volume Measurement and Point Cloud .....	49
Figure 26. AutoCAD Civil 3D Point Cloud Display and TIN Surface .....	50
Figure 27. Georeferencing Point Cloud in Civil 3D.....	51
Figure 28. Borderline - Base 3D Surface Model .....	52
Figure 29. Z-value Estimation Surface Height - Pothole Depth.....	54
Figure 30. Grayscale Converted and Computed Gradient Magnitude.....	55
Figure 31. Watershed-based Segmentation Sample Result .....	56
Figure 32. Pilot Study Site 1: Tapestry Drive.....	57
Figure 33. Tapestry Drive: Point Cloud and Camera Setup – Top and Side View .....	59
Figure 34. Tapestry Drive: Annotated Potholes .....	60

Figure 35. Tapestry Drive: Orthomosaic and DSM.....	61
Figure 36. Tapestry Drive: Overlapping Images for the Orthomosaic .....	62
Figure 37. Tapestry Drive: Clipped Road and Pothole Data .....	63
Figure 38. Tapestry Drive: Point Cloud.....	64
Figure 39. Clipped Point Cloud: Sample 1, 2, 3 .....	64
Figure 40. Sample 1, 2, 3 Side View Before and After Filter.....	65
Figure 41. Sample 1 Point Cloud in Civil 3D.....	66
Figure 42. Sample 1 TIN Surface Layer .....	67
Figure 43. Sample 1 Base Surface and Pothole Surface Z-values .....	68
Figure 44. Sample 2 and 3 Z-values .....	69
Figure 45. Pilot Study Site 2: Colony View Drive .....	71
Figure 46. Colony View Drive: Point Cloud and Camera Setup - Top and Side View....	72
Figure 47. Colony View Drive: Annotated Potholes .....	73
Figure 48. Colony View Drive: Orthomosaic and DSM .....	74
Figure 49. Colony View Drive: Clipped Road and Pothole Data.....	75
Figure 50. Colony View Drive: Clipped Point Cloud Samples 1, 2, 3, 4.....	76
Figure 51. Colony View Drive: Sample 4 Side View Filtered .....	77
Figure 52. Colony View Drive: Sample 1 Point Cloud in Civil 3D .....	78
Figure 53. Colony View Drive: Sample 1 Z-value .....	79

## LIST OF ABBREVIATIONS

Digital Surface Model.....	DSM
Three-dimensional .....	DTM
Geographic Information Systems .....	GIS
Global Navigation Satellite System.....	GNSS
Global Positioning System.....	GPS
Inertial Measurement Unit .....	IMU
Kilometer .....	km
Light Detection and Ranging.....	LiDAR
Line-of-Sight.....	LOS
Meter .....	m
Miles per hour .....	mph
Point Cloud Library .....	PCL
Radio Detection and Ranging.....	RADAR
Red Green Blue.....	RGB
Robot Operating System.....	ROS
Scale Invariant Feature Transform.....	SIFT
Structure from Motion .....	SfM
Thermal Infrared .....	TIR
Three-dimensional .....	3D
Triangular Irregular Network.....	TIN
Two-dimensional .....	2D
United States Dollar.....	USD
Unmanned Aerial Vehicles.....	UAV

## **ABSTRACT**

### **UAV-BASED POTHOLE IDENTIFICATION: A PHOTOGRAMMETRIC APPROACH**

Jin Kyu Lee, M.S.

George Mason University, 2019

Thesis Director: Dr. Sven Fuhrmann

Roads and highways are the backbone of the US transportation system, allowing Americans to travel more than two trillion miles annually. But the conditions of the roads are deteriorating, as the need for transportation improvements far outpaces the amount of state and federal backlogs of road maintenance and repairs. In addition, it is becoming more expensive to maintain high-quality driving conditions because many of the roadways in the US were constructed in the 1950s and 1960s. Conducting routine maintenance and repairs of roads, such as fixing potholes and repaving roads are one of the most important task and priority for transportation authorities. In order to do so, road condition data is vital in transportation management. Over the last decades, significant advancements have been made and new methods and knowledge have been shared for efficient collection of road pavement data. This thesis investigates the utilization of small unmanned aerial vehicles (UAVs) like a Mavic 2 Pro for surveying and inspecting road surface conditions. The objective of this research is to identify potholes from UAV

captured images and create GIS datasets containing key information such as dimensions, severity level, and location of potholes. This paper will introduce five main methods for data collection, UAV image processing, dataset generation, 3D reconstruction, and feature detection. To test the feasibility of these methods, pilot studies are conducted in two different test sites located in Fairfax County, Virginia. Different flight parameters and environmental settings are examined to minimize technical errors and to build an optimal workflow that will provide the most accurate results. By using photogrammetry, GIS, 3D modeling, and image processing software, this workflow can be utilized by local transportation authorities to conduct quick surveys and evaluation of the roads while requiring minimal training and funding.

## CHAPTER ONE: INTRODUCTION

### **1.1 Introduction**

Americans rely almost exclusively on motor vehicles for mobility. Americans are driving more miles than ever before and the US Department of Transportation Beyond Traffic 2045 report issued in 2015 forecasts driving per capita remaining stable and overall driving increasing by 23 to 27 percent over the next 30 years, due to a rising population and more urban sprawl [1]. The U.S. road network connects Americans from across the country and safe, high-functioning roadways support freedom of movement and enable access to goods, services, and markets that are essential to the way of life of all Americans. Furthermore, roads make a crucial contribution to economic development and growth.

The highway system in the United States contains thousands of kilometers of pavements. These highways are typically made up of concrete, asphalt or other composite pavements ranging in condition, age and durability. In recent years, many road network maintenance programs were established in order to monitor and maintain the performance and condition of the road network, to predict future pavement conditions, and assess long term requirements and policies [2], [3]. Many programs established by the United States Department of Transportation are concerned with pavement data collection, performance database storage, pavement data analysis, data dissemination and

technology development for the road networks [4]. Pavement condition assessment is one of the key components in these programs. Pavement condition assessments requires reliable and accurate measurements on pavement surface distresses such as cracks, potholes, faulting, rutting, and etc. [5].

There are many factors that influence the quality and performance of a pavement. Traffic, moisture, subgrade, construction quality, and maintenance are the main factors of pavement deterioration [6]. Traffic is one of the most important factors influencing pavement deterioration, mostly caused by the number of load repetitions by heavy vehicles such as tractor trailers. Figure 1 shows an example of load distribution of asphalt and concrete pavement. The left graphic illustrates a rigid pavement – made up of concrete and the right graphic illustrates a flexible pavement – made up of asphalt.

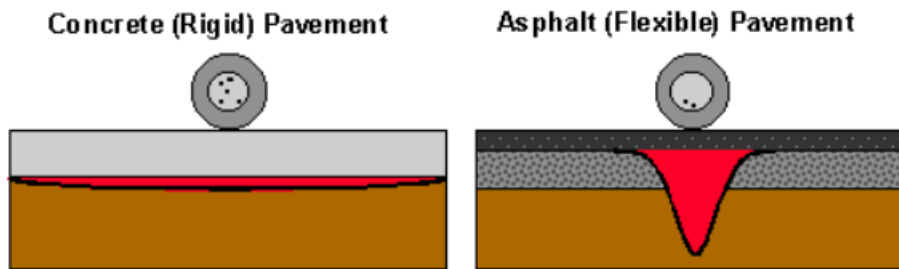


Figure 1. Structure of Concrete and Asphalt Pavement , American Concrete Pavement Association

Moisture can weaken the support strength of natural gravel materials. During the process of moisture ingress, sediments and particles beneath the pavement surface are lubricated. Therefore, losing the interlock structure, and subsequent particle displacement

resulting in pavement failure. Combination of traffic and moisture factors can be seen in Figure 2.

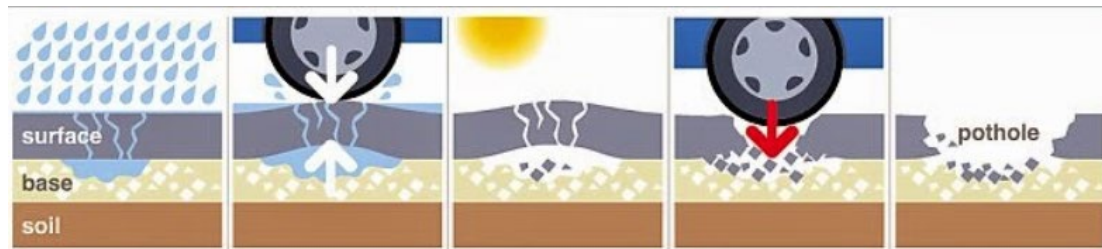


Figure 2. Different Stages of Pothole Development and Formation

The most common form of surface distress on concrete and asphalt pavements are potholes – bowl-shaped depression in the road surfaces. From a structural perspective, the development of a pothole starts when the small fragments of the road surface are dislodged and knocked out of the pavement layer. This distress will eventually progress downward into the lower layers of the pavement, eventually increasing in size. Additionally, potholes are caused by the expansion and contraction of ground water after the water has entered the cracks in old or weakened pavement. The water will soak up the mixture of rock, gravel, and sand and when the water freezes, the pavement expands, taking up more space under the pavement. This process causes the pavement to bend, break, and eventually erode parts of the pavement and develop potholes after many vehicles pass over the road. Potholes' minimum plan dimension is 150 mm and there are three different types of potholes: low-severity pothole (<25 mm deep), moderate-severity pothole (25 – 50 mm deep), and high-severity pothole (>50 mm deep) [7]. These three

different types of potholes can be seen in Table 1. In addition, potholes are important clues indicating structural distress of the road surfaces, and accurately identifying and detecting potholes is one of important tasks for determining appropriate maintenance and repair plans.

**Table 1. Common Pothole Severity Levels**

Pothole Severity Levels		
<i>Low</i>	<i>Moderate</i>	<i>High</i>
		
Most likely will not cause damage	May cause tire or rim damage	Will significantly damage to tires, rims, suspensions or axels

Most potholes would not occur if the root cause was repaired before the development of the potholes. Potholes are typically repaired by excavating and rebuilding, or patching. Timely repairing potholes is critical in ensuring the quality of the road, safety, and long-term cost of maintenance. Many research efforts have been made for developing a technology that can automatically detect and identify potholes [8]–[10], and these efforts contribute to improvement of survey efficiency and pavement quality, as well as the safety of drivers. In current practice, pavement image and video data collected by digital sensors are reviewed by experienced surveyors to manually detect and assess pavement defects. However, current manual detecting and evaluating methods are not only time-consuming but also limited by survey operating costs. To overcome these

limitations, several research efforts towards automating pavement distress detection have been undertaken. Existing research in pothole detection can be divided into three methods: vibration-based [11]–[13], 3D reconstruction-based [14]–[16], 2D vision-based [7], [9], [15]–[18].

Although these newer methods are advantageous over manual detection and evaluation methods, the new methods require more sophisticated equipment. As a result, these new pothole detection methods have proven to be computational heavy and expensive. This research will present a simpler and cost-efficient approach for automated pothole detection based on unmanned aerial vehicle (UAV) captured road surface images. These images are collected using a low-cost, consumer-grade drone, Mavic 2 Pro, and captured with mounted RGB color sensors. An example of these images is shown in Figure 3.

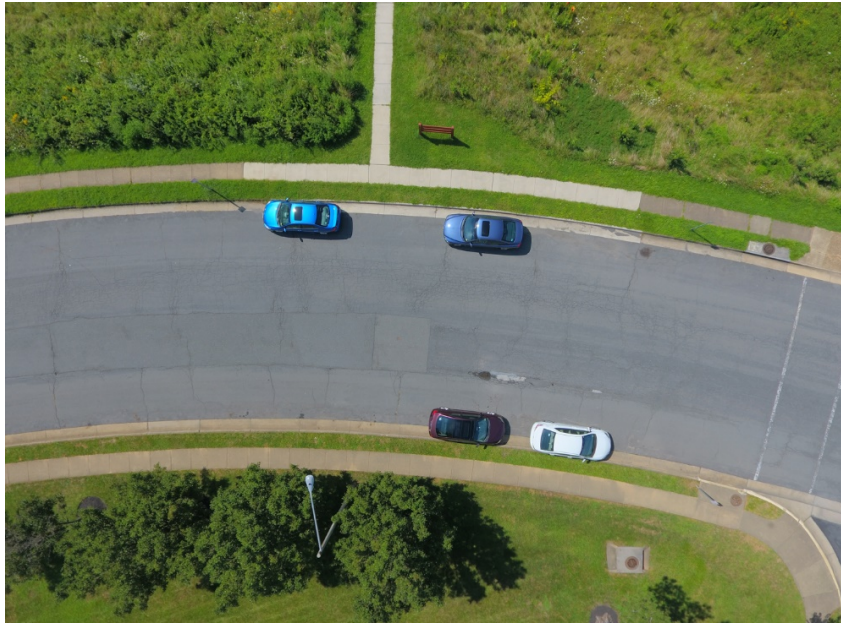


**Figure 3. UAV Captured Image**

One primary reason for using UAVs to collect road pavement data is that the operating cost of UAVs is cheaper than using experienced survey teams for manual collection. In addition, UAVs capture larger area than traditional vehicle sensors, and have higher spatial resolution than satellite images. Depending on the type and configuration of UAV, the acquisition cost might vary, however in the long-run having remotely sensed road pavement data is more cost-effective, time-efficient and safe as well.

### **1.2 Thesis Objectives**

The aim of this project is to research the applications of UAVs in collecting road surface condition data and to investigate how high-resolution UAV images can be utilized to improve and simplify current existing methods for evaluating and detecting potholes on pavements at a reasonable accuracy. Manual identification of potholes can be

done with UAV images. This can be seen in Figure 4. However, the goal of this research is to develop an automated detection system that can be implemented in different areas and at a larger scale.

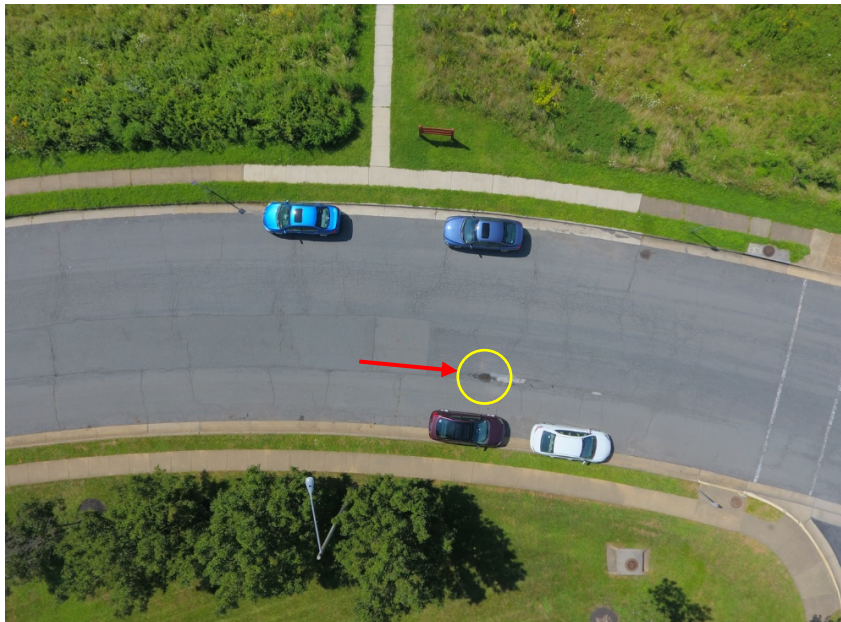


**Figure 4. Manually Identified Pothole**

In addition, the subobjective of this research is to examine different settings for flight operations such as altitude, sensor angle, and time to improve quality of the aerial image data. Different flight operations would yield different results in the later processing steps; therefore, it is critical to determine the optimal flight environment.

Essentially, the aim of this thesis is to investigate the feasibility of detecting potholes and the measurement accuracy of the potholes. Because 2D image processing technique would have difficulties finding the z-dimension (height) measurement of the

pothole, 3D reconstruction modeling techniques will be used in the research. The central objective and contribution of this study is to examine the feasibility of the proposed methodology and offer a simple tool for detecting and identifying potholes on road pavement and improve the efficiency of road maintenance practices.

Experiment results will demonstrate that the system will be reliable and practical for road pavement surveying and distress/anomaly detection that provides accurate results that can be used to improve pavement management systems and in the decision-making process.

### **1.3 Thesis Organization**

This paper is organized as follows. After this introduction section, Chapter 2 will introduce a general overview of pavement condition assessment system and a review of different pothole detection systems and sensors. Chapter 3 will introduce a proposed method and a pilot study which will include an overview and the workflow of the small experiment. Next, collected information from pilot study experiments will be used to refine data collection and processing steps. Finally, a 3D-based detection methodology will be proposed. Chapter 4 will provide a sample result from the initial pilot study with a detailed quality summary. Chapter 4 will also include a report on key findings as well as limitations of first proposed approach.

## **CHAPTER TWO: BACKGROUND AND LITERATURE REVIEW**

The first section of this chapter will include background information on different pavement composition and structure, different types of distresses, and process of pavement condition assessment. Next section will briefly explain existing methods for pavement distress detection. Last section of this chapter will include some information on UAVs and related fields such as remote sensing and photogrammetry.

### **2.1 Pavement Condition Assessment**

There are three components for the process of pavement condition assessment: data collection, distress identification and defect assessment [4]. In current practice, these processes are to a large extent manually conducted. The first process typically uses digital inspection vehicles to collect pavement data, using several sensors such as optical sensors for surface imaging, laser sensors for measuring depth and height, accelerometers for roughness measurements, and laser scanners for longitudinal and transverse scanning [9].

Pavement distresses are defects visible on the pavement surface and they are signs of deterioration such as cracks and potholes [5], [21]. Traditionally, the optical sensor captured data such as video and image data are evaluated by technical experts who manually detect and visually assess pavement defects on their computer screens. Their judgement is based on their knowledge and experiences. In addition, a standard distress manual is used to define different levels of severity, required action and extent for each

categories of distress [2], [7]. Typically, manual pavement inspections are conducted without any digital sensors using a van or minivan at a speed of 8 to 15 mph in addition to using data collection software [22]. Many of the transportation agencies use commercial data collection software and these do not support the automated detection of distresses like potholes and patching. An example of Pavement Condition Assessment software by ARRB Group Inc. is shown in Figure 5.

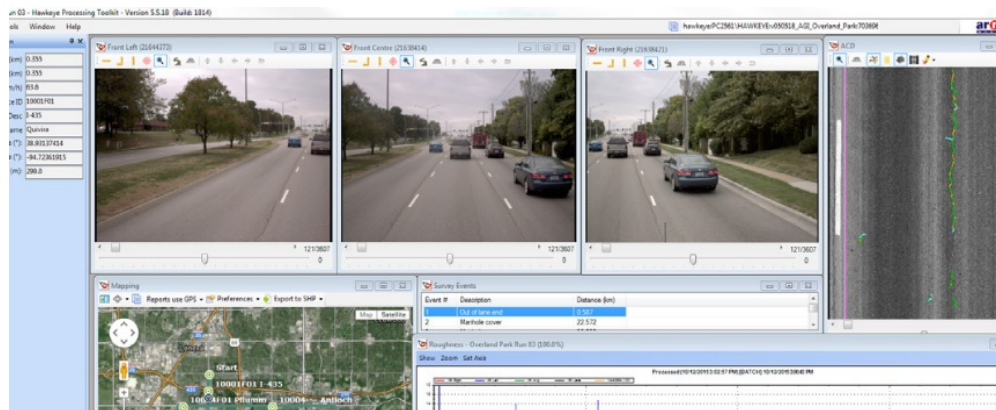


**Figure 5. Pavement Condition Assessment Platform**

The overall goal of pavement condition assessment is to collect pavement data, identify pavement distresses and assess the health of pavement layer. One of the most common pavement distress is a pothole. Potholes are bowl-shaped depressions of various sizes in the pavement surface [7], [22]. Their visual characteristics can also be defined as almost circular and elliptical shaped regions in the pavement surface. Additionally, potholes are partially surrounded by a dark shadow due to depression and depth and have granular and coarse textural appearance due to deterioration and fragmentation in the

pavement surface. Based on these visual characteristics, manually identifying and assessing the potholes using image and video data is tedious and time-consuming for transportation agencies; This is the main reason why many transportation agencies only conduct pavement condition assessment annually [2].

These limitations raise a need for automation and improvement of pavement condition assessment processes. Therefore, this research will explore existing pavement condition assessment methods and develop a new pavement distress detection system which can automate the process of pavement surface data collection, pothole detection, identification and classification, and create accurate locational/positional information on the potholes using geographic information systems.

## **2.2 Existing Pothole Detection Methods**

### **Vibration-based**

Vibration-based approaches use accelerometers and mobile phone sensors to detect potholes [11]–[13], [23]. Yu and Yu proposed a vibration-based approach using accelerometer to evaluate pavement conditions [11]. This vibration-based system “feels” the surface condition based on mechanical response of the testing vehicle, shown in Figure 6.

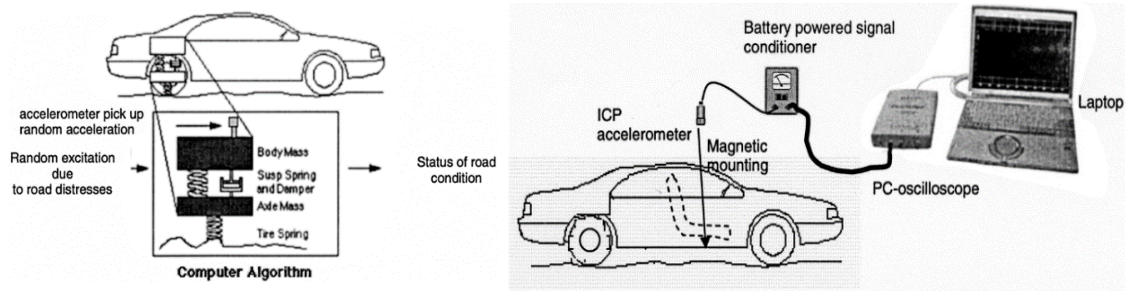


Figure 6. Vibration-based System Schematics

In addition, the recorded interactions of the surface and vehicle can estimate or “detect” the distresses of pavement including cracks and surface rutting, based on impact forces on the driving vehicle. Using this testing system and data was collected to validate the measurement and recorded signals enable the estimation of road condition. Graphical example of vertical acceleration records indicating vibration is shown in Figure 7. The acceleration records indicate (a) small vibration: idle of the engine; (b) medium vibration: good road condition; (c) high vibration: poor road condition

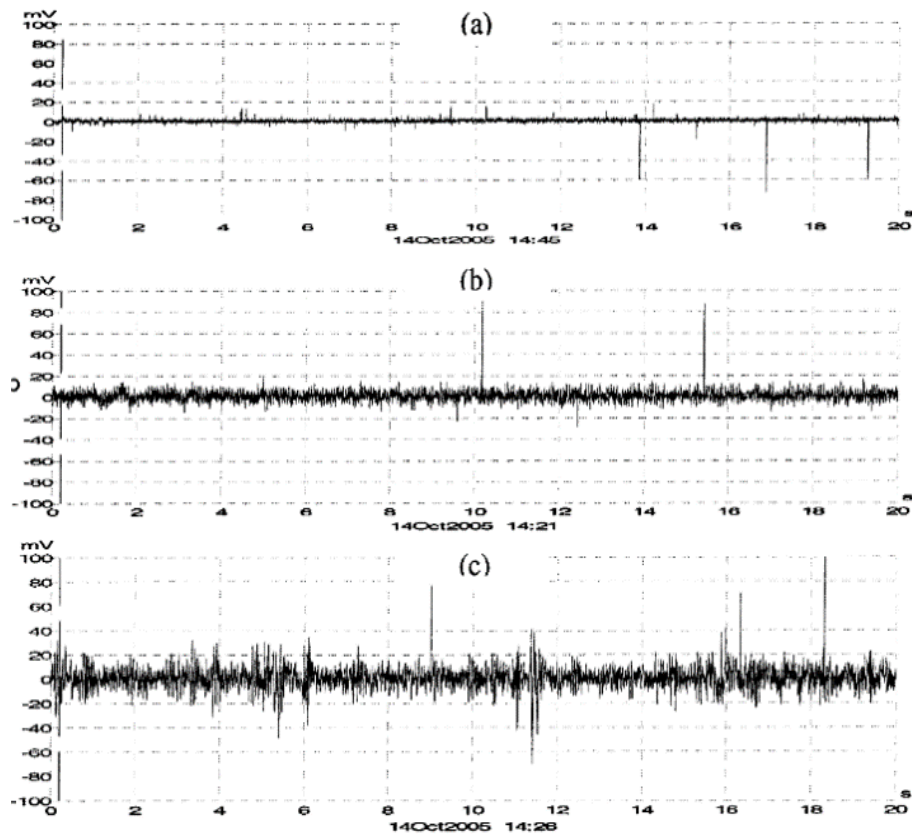


Figure 7. Acceleration Records

Unlike other following methods, a vibration-based system has the advantage of small storage requirement, cost-effective and amenable for automatic real-time data processing [11]. It is important to note that limitation of this method is that it does not provide the complete visual details of distress characteristics as by image and video-based system. Image and video-based systems however require large storage space and extensive computation power for image processing.

## 2D Vision-based

2D vision-based approach is based on image or video data. The image approaches are mainly focused on pothole detection using image processing techniques, such as

image segmentation, shape extraction, identification and extraction, and etc. [8], [19], [24]–[27]. Most common steps of 2D vision-based methods are divided into three steps: 1) image segmentation – shape and texture extraction 2) candidate region extraction, and 3) decision – pothole detection (Figure 8).

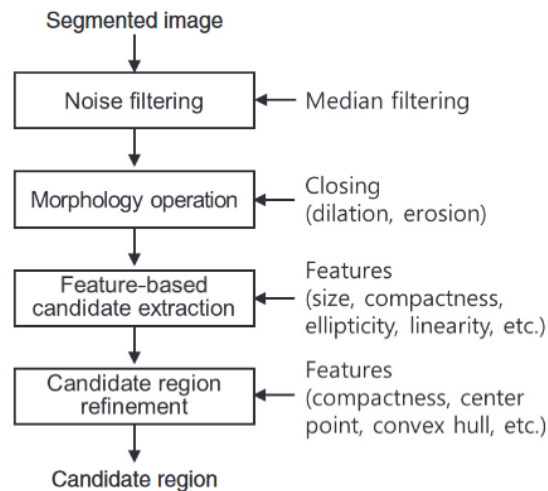


**Figure 8. 2D-based Detection Method Workflow**

Akagic et al. developed an efficient unsupervised 2D vision-based method for pothole detection without the process of training and filtering. The method starts with extracting asphalt pavements by analyzing RGB color space and using image segmentation. This determines the road pavement – region of interest, the area on which potholes can be found. Once the asphalt in the region of interest is accurately detected, the asphalt pavement images are used with Otsu thresholding and spectral clustering for eliminating all linear and image boundary shape and resulting in the detection of nonlinear shapes, i.e. pothole. The advantages of 2D-vision based approach are detection

and evaluation of pavement distress is less expensive and time-consuming than manual detection and evaluation methods. In addition, two-dimensional images can accurately detect a pothole, while manual detection is prone to human error. 2D-vision based methods are limited to a single frame. Other 2D-vision based method such as video-based approach can overcome the single frame limitations. Video-based approaches are used to not only identify and recognize potholes but also calculate the total number of potholes over a sequence of frames and video clips [28], [29].

### **3D Reconstruction-based**

Typical 3D reconstruction-based detection methods rely on 3D point clouds, provided by laser scanners or by stereo-vision algorithms using a pair of digital sensors [15], [30], [31]. In addition, 3D reconstruction methods can be further classified into 3D laser scanning methods [14], [32], [33] and visualization using hybrid systems such as Microsoft Kinect sensors that uses digital cameras to capture consecutive images of lines projected by infrared lasers [34], [35]. Zhang et al. developed an automatic pavement defect detection system using 3D laser scanners installed on a vehicle. The 3D pavement data collection and measurement system can be shown in Figure 9.

Above automatic method used 3D laser scanning pavement data and detected pavement cracks and pavement deformation defect information. Experimental tests were conducted using a sparse processing algorithm, which was designed to obtain 3D pavement profiles and extract crack candidate and deformation points. The results showed that 3D laser profile detection method can effectively detect most cracks under different environment and surface conditions. The accuracy of detection was above 98%.

Furthermore, the method was also able to accurately detect different categories of deformation defects such as potholes, shoving, and rutting. Below figure illustrates 3D installed collection sensor (right) and measurement system (left) [14]



Figure 9. 3D-based Collection Measurement System

### **2.3 Unmanned Aerial Vehicle Systems**

This section discusses the definition and background of the UAVs in this research, the evolution and state-of-the-art of the use of UAVs in the field of remote sensing and photogrammetry from different communities. In addition, this section provides information on the utilization of UAVs in remote sensing methods and other related techniques such as photogrammetry for geographical data processing and analysis. Most of the UAVs used as remote sensing and photogrammetric platforms are equipped with highly accurate hardware such as a global navigation satellite system (GNSS) such as GPS for tracking flown paths and recording x, y, z data during image captures, an electronic compass, barometric pressure sensors for altitude and an inertial measurement unit (IMU) to estimate the UAV orientation within 1-2 meters in position

and 1-2° orientation accuracy [36]. The applications of UAVs have grown considerably over the last decade with rising number of researches in UAV-based remote sensing and photogrammetry.

### **UAV Overview**

In this research unmanned aerial vehicle systems will be referred as UAV(s) and drones since “UAV” and “drones” are the most popular terms in both literature and in practice. The earliest recorded use of a UAV dates back to 1849 when the Austrians attacked the Italian city of Venice using unmanned balloons that were loaded with explosives [37], [38]. Although this balloon “UAV” is not considered as a UAV nowadays, its aerial technology and unmanned nature is similar to the currently existing UAVs.

Recently, the use of UAVs has become mainstream in many applications/fields and easily accessible to everyone. As a result, the safety concern appeared and regulations were put in place to limit the flight operations of UAVs by civilians, mostly. Many civil aviation authorities from many countries implemented rules and regulations to reduce the number of accidents at both air and ground space level. Most of these authorities provide certification exams to help improve technical and situational skills of UAV operators. Common rules of UAV use, around the world, are as follows:

- Restricted to flights within line-of-sight (LOS) of an operator and an observer(s).
- UAVs cannot be flown in restricted airspaces, such as airports and military airspace.
- UAVs cannot be flown above certain altitude (different for every country).

In addition, a few common UAV categories/classification are described in Table below. Table 2 includes the main characteristics of small and micro UAVs and different specifications for each UAV category/class [39]. Below are the examples of commonly used UAS for remote sensing.

**Table 2. Common UAS for Remote Sensing**

Name	Manufacturer	Weight (kg)	Endurance (h)	Integrated payload (i) or Payload weight (w)
<i>Common fixed-wing unmanned aircraft</i>				
SwingletCAM	SenseFly	0.5	0.5	(i) 16 Mpx RGB camera
GeoScan101	GeoScan	2	1	(i) 24.3 Mpx RGB camera
UX5	Trimble	2.5	0.83	(i) 16.1 Mpx MILC RGB camera
Pteryx	FotoMapy	5	2	(w) 1 kg w/o batteries
Sirius I	MAVinci	3	0.91	(i) 16 Mpx RGB camera
Kahu	Skycam	4	2	(i) Double-head 16 Mpx MILC RGB cameras
<i>Common rotary-wing unmanned aircraft</i>				
Geocopter	IGI	90	2	(w) 30 kg
Scout B1-100	Aeroscout	75	1.5	(w) 30 kg
R-MAX, type II	Yamaha	100	1	(w) 28 kg
<i>Common multi-rotor unmanned aircraft</i>				
md4-1000	Microdrones	3	1.46	1.2 kg
HT-8-2000	Height-Tech	2.4	0.28	2 kg
Aibot x6	Aibotix	2.4	30	2.5 kg
Falcon 8	Ascending technologies	1.45	0.33	0.75 kg
HexaKopter	MikroKopter	1.2	0.6	1 kg

Above UAVs are commonly used for different remote sensing applications. Furthermore, some common drone models available for average consumers are listed and shown in Figure 10 below:

- a) 3DR Solo
- b) Parrot ANAFI
- c) DJI Phantom and Mavic
- d) Microdrones MD4-200
- e) Sensefly eBee X



**Figure 10. Consumer-grade UAVs: Left to Right (a) – (e)**

Lastly, the main components of UAVs include: body (form factor), power supply (batteries), system hardware (flight controller), sensors (payload), actuators (motors and propellers) and flight stack (firmware, middleware, operating system and software).

### **UAV Remote Sensing**

The emergence of UAV remote sensing has proved a cost-effective and efficient alternative to traditional remote sensing techniques and this technology has been

researched, and applied successfully in many different applications such as land surveying and mining, ecological and environmental [40], infrastructure inspection, forestry and agriculture [41], archaeology and cultural heritage, traffic monitoring, and 3D reconstruction modeling [42]. UAV-based remote sensing has become a powerful tool that can be used remotely sense relatively small spatial extent. In addition, UAV-based remote sensing has the capability to provide data at high temporal and spatial resolution. These remote sensing platforms and equipment play a key role in how data is collected. For example, based on this research theme, the most commonly used platforms for pavement data collection are land-based surveying vehicles. However, the limitations of land-based surveying vehicles have small coverage and can only capture a small portion of the scene at a time. In order to capture larger pavement roads, UAVs can be and has been introduced in this field. Although many transportation agencies still use land-based vehicles, flexible UAV platforms are being developed more in the pavement management field. Furthermore, UAVs can have different sensor configurations and mount different types of sensors such as LiDAR, multispectral, RADAR, optical, and others to collect many forms of remote sensing data.

### **UAV Photogrammetry**

Traditional method of pothole detection uses digital images and videos with single band or RGB data to automatically detect pavement damages. In addition, image processing and machine learning methods are most commonly used and are often

combined to extract features of pavement defects [43], [44]. Although these methods are commonly used to process aerial image data, other remote sensing related technique can be used to improve the analysis of UAV image data. Since UAV image data offers high spatial resolution, photogrammetric methods can be used to reconstruct the scene of the UAV image data in 3D and acquire more accurate data, which is represented in points in this method. Typically, photogrammetric data processing generates geo-referenced 3D point clouds from unsorted, overlapping, and aerial image of the ground surface. There are different algorithms such as Structure from Motion (SfM) and Scale Invariant Feature Transform (SIFT).

Uses of UAV photogrammetry method for surveying and collecting point cloud data can be seen in many past researches. Typically, UAV-based photogrammetry uses a LiDAR sensor, mounted on an UAV, to map the overflown environment in point clouds. One research was using UAV for mapping and textural analysis of agricultural fields. The LiDAR point clouds were collected and recorded, mapped, and analyzed using the Robot Operating System (ROS) and the Point Cloud Library (PCL) [45]. This thesis research will also similar methods and equipment for road surveying application and measure height estimates of the identified potholes. In this aspect, the use of UAV-based photogrammetry with the support of remote sensing and computer technologies is clear and beneficial to survey efforts and could also be applied to road surveying application as well.

Past researches show that many forms of remotely sensed data and 3D point cloud generation algorithms have been developed in many different fields [46]–[52]. In this

aspect, Light detection and ranging (LiDAR) sensors are used to acquire the elevation data of the pavements to measure the differences in height to identify deteriorated surfaces such as potholes. In addition, other sensors such as radar can be used to detect voids, cracks and material properties by penetrating the ground of the pavements [53].

## CHAPTER THREE: DATA AND METHOD

This chapter elaborates the equipment, data, method, and process for each step of the thesis workflow. Each section of this chapter systematically details every action performed during the pilot study and experiments. The main method employed in this study to develop and evaluate the feasibility of the three research objectives: identifying potholes, generating pothole data, and evaluating the flight settings for UAV road surveying. This main method is divided into four major steps. The chapter is organized as follows: Section 3.1 Overview presents a general overview of the equipment, tools and software, field experiments, and workflow steps; Section 3.2 Equipment and Tools details the equipment, software, and other tools used to conduct pilot study and process experiment data; Section 3.3 Pilot Study specifies the procedures used for UAV survey flight operations; Section 3.4 Data Processing explains different steps of preprocessing and cleaning up the data that will be used in the following sections. The last three sections: 3.5 GIS Development, 3.6 3D Reconstruction, and 3.7 Image Processing Detection details the input and output data, and workflow procedures to accomplish each objectives.

### **3.1 Overview**

The methods employed in this study to develop and evaluate the feasibility of the three objectives were constructed and refined through iterative processes and pilot

studies. The accessibility of consumer-level UAVs such as DJI Mavic 2 and Phantom 4 are advantageous to nearly all other industry- and commercial-level UAVs due to their const. Mavic 2 costs \$1,499 USD and have the capability to operate up to 31-minute flight time, 11-mile (18 km) flight distance with no wind and at a consistent 15.5 mph (25 km/h) speed in regular flight mode. Detailed technical specifications such as aircraft diagram, flight modes, transmission links, and sensor camera information of Mavic 2 are listed in Section 3.2 Equipment and Tools.

For processing the surveyed UAV images, commercial- and professional-level software such as Pix4D's Pix4Dmapper, ESRI's ArcGIS 10.6.1, and Autodesk's Civil 3D were used. Alternatively, a few opensource software such as CloudCompare, Point Cloud Library (PCL), MeshLab, QGIS, and VisualSFM were also evaluated to compare the output and result quality, user-friendliness and usability as well.

Pilot study and research experiments were conducted in four different locations. These locations were all located in Fairfax County, Virginia. The locations were determined as optimal spots or roads for surveying due to the relatively low traffic flow and tall obstacles which made it easier to survey the road and potholes, measure ground truth data, and operate UAV for aerial image collection.

After the pilot study and field work, captured aerial images needed to be processed, cleaned, and exported in different file format types. First Pix4Dmapper, a photogrammetry software was used to process the images from different survey sites into new data types such as .geotiff raster, .las point cloud, and .fbx texture mesh data. Raster data were used then used as inputs in ArcMap for creating GIS datasets of potholes with

attributes containing critical information about each pothole. Point cloud data were used to construct 3D models of the potholes and to obtain height/depth information of the pothole. Clipped images of the roads were then used as inputs in MATLAB to test an image processing method called Marker-Controlled Watershed Segmentation to separate potential pothole objects from other objects in the images.

### **3.2 Equipment and Tools**

The equipment, software and tools used for the data capture, photogrammetry processing, GIS development, and 3D modeling portion of the thesis encompass three items: UAV – DJI Mavic 2 Pro, Pix4D – Pix4Dmapper, Autodesk – Civil 3D, MathWorks – MATLAB, and a personal workstation. The main aerial vehicle used in this research: Mavic 2 Pro is illustrated in Figure 11 diagram.

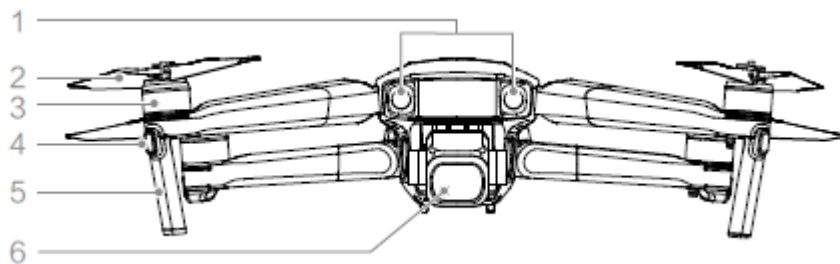


**Figure 11. Mavic 2 Pro Aircraft Diagram**

1) Forward Vision System: one of the Vision Systems that provided omnidirectional obstacle sensing and create a real-time map of its flight route as it flies which can be used for Failsafe Return to Home function, 2) Propellers: used four low-noise propellers 3) Motors: attached and removed propellers, 4) Front LEDs: used for

safety, showing the orientation of the aircraft, 5) Antennas: transmitted signal between the aircraft and the remote controller, 6) Gimbal and Camera: used Hasselblad L1D-20c camera. More detailed specifications can be seen in Table 3. The decision of using Mavic 2 Pro was made based on its high maneuverability characteristic and omnidirectional obstacle avoidance ability. These factors made Mavic 2 Pro more versatile and reliable than other drones which are typically bigger than Mavic 2 Pro in size.

**Table 3. Detailed Mavic 2 Pro Specifications**

<b>Aircraft Specifications</b>	
Dimensions	Folded: 214×91×84 mm (length×width×height) Unfolded: 322×242×84 mm (length×width×height)
Max Speed (no wind)	72 kph (Sport-mode)
Max Flight Time (no wind)	31 minutes (at a consistent 25 kph)
Max Flight Distance (no wind)	18 km (at a consistent 50 kph)
Max Wind Speed Resistance	29–38 kph
Operating Temperature Range	-10°C to 40°C
Operating Frequency	2.400 - 2.483 GHz 5.725 - 5.850 GHz
Takeoff Weight	907 g
Internal Storage	8 GB
External Storage	Micro SD™ Supporting Micro SD with capacity up to 128 GB and R/W speed up to UHS-I Speed Grade 3
Global Navigation Satellite System	GPS+GLONASS
<b>Obstacle Sensing Systems</b>	
Forward Vision System	Precision Measurement Range: 0.5 - 20 m Detectable Range: 20 - 40 m Effective Sensing Speed: ≤ 14m/s FOV: Horizontal: 40°, Vertical: 70°
Backward Vision System	Precision Measurement Range: 0.5 - 16 m Detectable Range: 16 - 32 m Effective Sensing Speed: ≤ 12m/s FOV: Horizontal: 60°, Vertical: 77°
Upward Vision System	Precision Measurement Range: 0.1 - 8 m
Downward Vision System	Precision Measurement Range: 0.5 - 11 m Detectable Range: 11 - 22 m
Side(s) Vision System	Precision Measurement Range: 0.5 - 10 m Effective Sensing Speed: ≤ 8m/s FOV: Horizontal: 80°, Vertical: 65°

<b>Camera</b>	
Sensor	1" CMOS Effective Pixels: 20 million
Lens	FOV: about 77° 35 mm Format Equivalent: 28 mm Aperture: f/2.8–f/11 Shooting Range: 1 m to ∞
ISO range	Video: 100-6400 Photo: 100-3200 (auto) 100-12800 (manual)
Shutter Speed	Electronic Shutter: 8–1/8000s
Image Resolution	5472×3648
Video Resolution	4K: 3840×2160 24/25/30p 2.7K: 2688×1512 24/25/30/48/50/60p FHD: 1920×1080 24/25/30/48/50/60/120p

During the initial stages of this research and experiments, many software and tools were tested to see which ones would be most suitable for photogrammetry processing (point cloud, raster, orthomosaic generation), GIS development (spatial dataset generation), 3D modeling (textured mesh generation), and image processing (pothole detection) steps. The first step of this research was to process the collected drone images. In order to do so, the best photogrammetry software needed to be used. Out of many other photogrammetry tools and software, Pix4D was picked. Pix4D is one of the most widely known companies in the photogrammetry, industry-grade level survey, and 3D mapping fields. In addition, Pix4D's solution can be used on desktop, cloud, and mobile platforms, making it easier for consumers to access mission planning, data processing and sharing tools in online and offline environments. Pix4Dmapper software used photogrammetry and computer vision algorithms to transform RGB, thermal infrared (TIR), multispectral (MSS) band images [54]. In addition, Pix4Dcapture, a phone

application, can be used to plan flight missions for drone surveying and it is a free application that can be used with nearly all DJI drones and Parrot drones. Pix4Dmapper software and Pix4Dcapture application's main screen can be seen in Figure 12

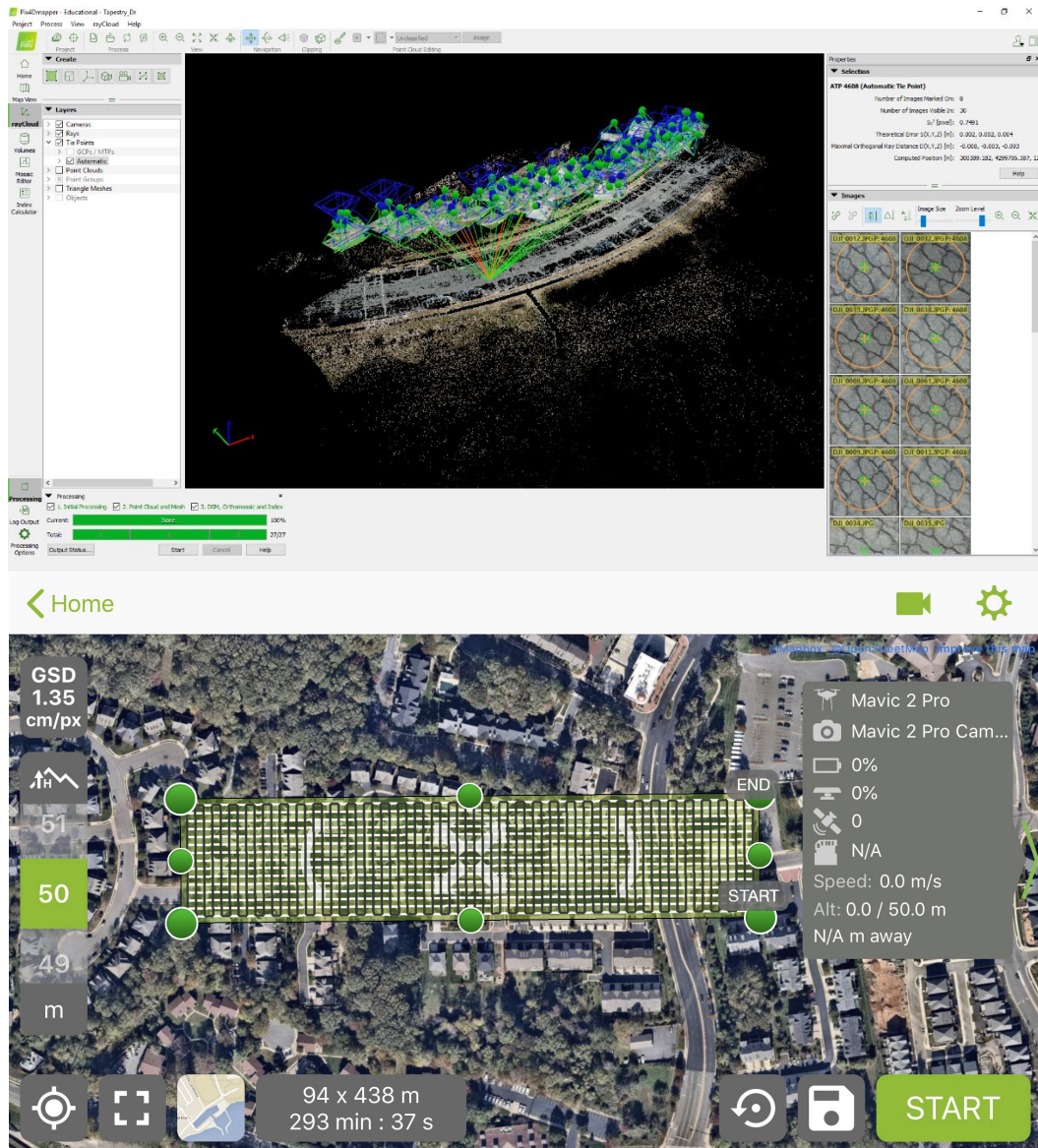
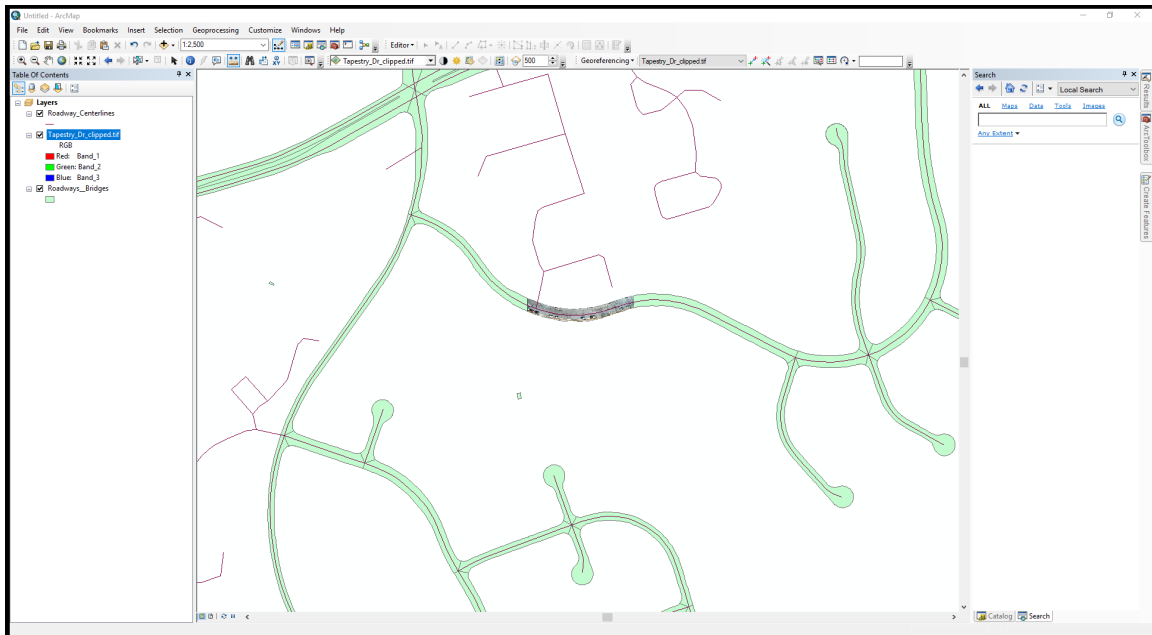


Figure 12. Pix4Dmapper and Pix4capture Screen

For the GIS development stage, ESRI's ArcMap 10.6.1 was used to process the orthomosaic image. ArcMap's alternative QGIS could be used for the GIS development as well. However, due to the wide-usage of ArcMap by local government authorities, ArcMap was chosen as the main GIS software that will be used in this research. Orthomosaic image loaded in ArcMap along with Fairfax County GIS data can be seen in Figure 13.



**Figure 13. ArcMap 10.6.1 with Main Data**

Next, to construct 3D models using point cloud data and to create TIN surface models to measure the elevation of the potholes, CloudCompare v2.11 alpha, Autodesk's ReCap Pro and Autocad Civil 3D was used. CloudCompare is a 3D point cloud and triangular mesh editing and processing software. CloudCompare's graphical user

interface is depicted in Figure 14. The main entities in CloudCompare are divided into three different groups: Point Cloud, Mesh, and Polyline. Point Cloud group is typically a set of 3D points (x, y, z) and can be associated with RGB colors. Mesh group is a set of triangles, which are represented by triplets of integer indexes. These integer indexes are relative to an associated cloud, or the mesh vertices, meaning a mesh inherits of all the features associated to a point cloud. In CloudCompare, a polyline is a set of points connected by contiguous segments and internally, a polyline is a set of indexes. These indexes, similar to the mesh indexes, are associated with a point cloud. These indexes or vertices are also stored as a point cloud, and they are generally a child of the mesh object in the database tree. Polylines are recognized as 3D objects, but they can also be 2D entities as well.

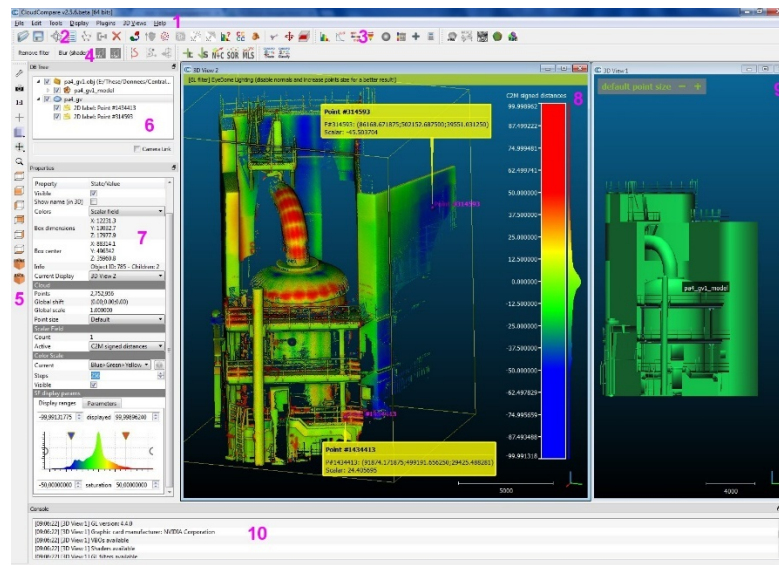


Figure 14. CloudCompare Graphical User Interface

For the other 3D reconstruction steps such as 3D point cloud conversion process and TIN surface model creation process, Autodesk ReCap Pro and Civil 3D was used. ReCap Pro was used to convert noise filtered and segmented point cloud data (.las format) from CloudCompare to Autodesk Civil 3D readable point cloud data (.rcs format). More details on the usage of ReCap Pro and Civil 3D can be found in 3.6 3D Reconstruction section. For the image processing step, MATLAB was used to test existing feature detection algorithms such as edge detection and segmentation method to test the feasibility of image processing methods in detecting potholes from aerial images.

The workstation used in this research project is a custom-built desktop, which contains an Intel Core i7 7700K CPU @ 4.8 GHz, 32 GB DDR4-2132 RAM, NVIDIA GeForce GTX 1080 Ti GPU, 1 TB SSD, and Windows 10 Pro Operating System.

### **3.3 Pilot Study**

To test the feasibility of the proposed method, pilot studies were conducted in two different locations. The locations of test sites were Colony View Drive and Tapestry Drive in Fairfax, Virginia (depicted in Figure 15).



**Figure 15. Pilot Study Test Sites**

The objective of the pilot study was to test different settings for flight operation, such as altitude, sensor angle, operation time, image overlap percentage, and flight path. Test studies were performed in a near-optimal, accessible, safe environment. Although the test sites were all located on local roads, this research should be applicable to all classes of roads. An overview of the pilot study process is depicted in Figure 16. This workflow illustrates the collection of ground truth data and flight planning process.

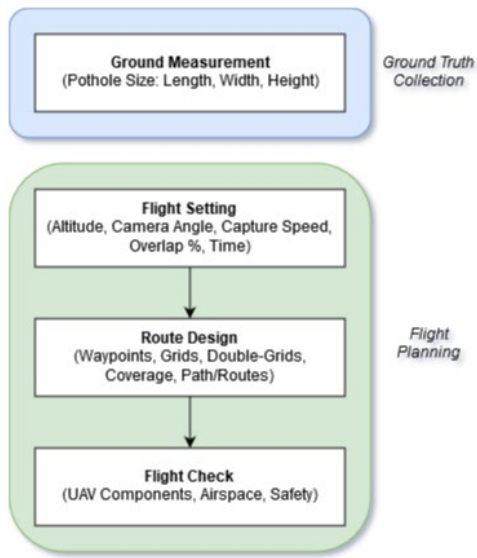


**Figure 16. Pilot Study Process**

One of the most important tasks in surveying using drones was flight planning and logging, and refining flight settings. During the pilot study process, UAV surveying on the test site roads required certain flight settings and environmental conditions to be met. Before starting the survey mission, the drone’s flight setting such as altitude, overlap, camera angle, and capture speed needed to be optimal for each test site. Naturally, the three pilot study sites had different environmental factors, obstacles, land characteristics; therefore, it was critical to change the flight settings at each location. Before aerial surveying took place, the height of the surrounding obstacles such as tall trees, light poles, and utility poles needed to be examined. By evaluating nearby obstacles and height information, the optimal altitude for flying on pilot study sites was determined. This allowed safer in-flight operations and reduced the risk of crashing the drone. Capture speed was set to medium by default because there were many other overlapping images that would compensate for the slightly blurred aerial images. Capture

speed factor was not much of a significant factor in flight planning because the only major impact it had on the flight operation was either increased flight time or reduced flight time. Next, two image-overlap settings were adjusted. The front overlap which sets the frontal overlap between consecutive images along a flight line was set to 80%. The side overlap which sets the side overlap between images from adjacent flight lines was set to 80% as well. The reason behind selecting 80% overlap was 60-70% of image overlaps produced significantly lesser quality point cloud data during photogrammetric processing step than 80%. In addition, going over 80% was not necessary because setting 80-90% image-overlap increased the time of photogrammetric processing and computing time. The results of 80-90% image-overlap aerial images did not necessarily improve the quality of the output point cloud data because the consecutively captured images were almost identical with each other. The initial photogrammetric image calibration and keypoint matching process took longer and the quality did not improve significantly due to the images being too identical, which goes against the theory and mathematical concept of photogrammetry, where you have two different side images with some overlapping parts in the two images. As mentioned earlier, the percentage of image-overlap settings also affected the total time of the flight operation. Flight operation time was longer when the image-overlap percentage was higher, and flight time was shorter when the image-overlap percentage was lower. These two factors were inversely related. Flight time was also affected by route designs, based on different patterns such as grid, double grid, waypoints, and orientation of the flight path.

Different route design patterns and paths were tested during the pilot studies. Route designing was also an important factor to flight planning because the path and patterns determined how long the aerial survey was going to take, and at what angle the camera needed to be set up. First, route design patterns affected the decision making of camera angle values. For example, when the flight path was a straight-path pattern and parallel to the road, the camera angle was set to 35°-45°. This technique helped acquiring higher resolution point cloud data, making potholes more distinguishable due to the shadow of the slope and elevation difference between regular road and potholes. When the flight path was a grid-path pattern, the camera direction was mostly perpendicular to the road and took images from the side of the roads. Grid-path pattern also collected similar images to the straight-path pattern.

This comparative experiment showed that the quality of output data such as point cloud data is ultimately dependent on the number of captured images. Grid-path pattern flight captured more images and thus provided higher spatial resolution. Higher spatial resolution data was directly related to having higher point density (points per unit area) output, and by having higher quality point cloud dataset, grid-path pattern flights produced higher quality 3D textured mesh during the 3D reconstruction step as well. Overall, it was difficult to distinguish whether a straight-path pattern or a grid-path pattern provided higher quality images since the main differences between the two was the number of images captured and the number of point clouds. Although the latter pattern provided higher resolution and more point cloud data, the flight time increased as well. Flight time had to be considered and therefore choosing the right or “optimal”

pattern was one of the most difficult tasks while conducting pilot studies. Pilot studies at two different locations were conducted and these experiments concluded that flight planning settings and route designs always changed and were different because of surrounding environmental conditions and factors.

Next important task in the pilot study was to collect ground truth data measurement of potholes. This ground truth data included length, width, and height information. This information was measured and recorded using laser distance measurer along with measuring tape and rulers. Although these tools were not industrial-grade measurement tools, combining the three tools and taking the average value of each length, width, and height size provided more accurate and consistent ground truth measurement data. An example of ground truth measurement can be seen in Figure 17.



**Figure 17. Example of Ground Truth Measurement Tools**

Once the potholes were sampled and recorded, potholes were annotated in QGIS to create basic map layers with pothole sample labels. The map layers with sample labels

were then exported as just an image, which was used as reference maps of pothole locations (Figure 18). These reference maps with pothole ground truth data were tested against the accuracy of the final processed data such as orthomosaic image, point cloud.

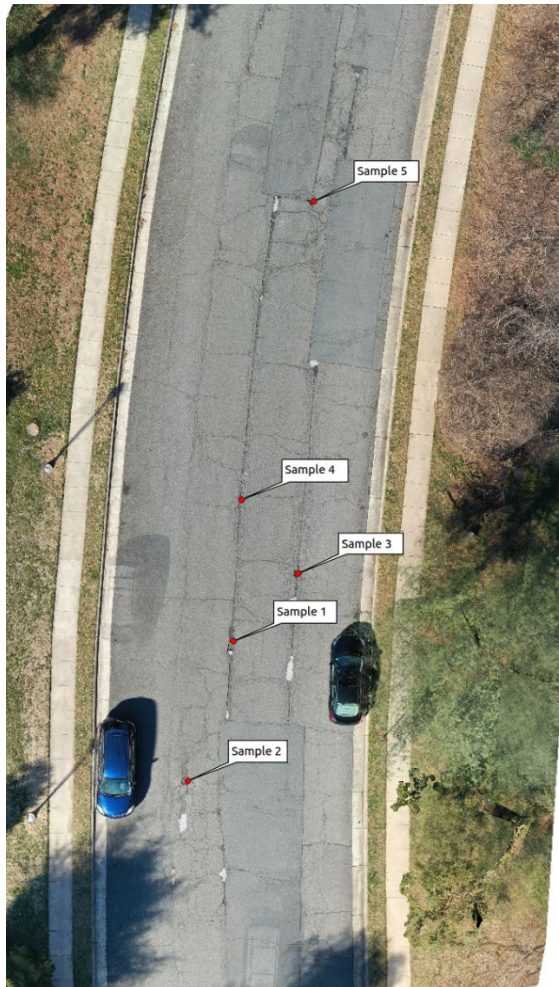


**Figure 18. Pothole Samples with Ground Truth Data**

### **3.4 Data Processing**

Once aerial images were captured and transferred to the main workstation, the images were compiled. First, drone captured images were uploaded to Pix4Dmapper photogrammetry software. Pix4Dmapper automatically detected the datum and coordinate system, geolocation and orientation of the images based on the captured images' EXIF data which was comprised of a range of settings such as ISO speed, shutter speed, camera model, image captured time, date and time, lens type, and GPS coordinates. The setting factors and parameters for this data preprocessing step are divided into three sections: 1) Keypoints Image Settings: Scaling → Matching → Calibration, 2) Point Cloud and Mesh Settings: Point Cloud Densification → 3D Texture Mesh Generation, 3) DSM/DTM and Orthomosaic Settings: Raster DTM, Raster DSM Filter and Generation, Orthomosaic Generation → Output File Format Selection. The processing options can be seen in Figure 19.

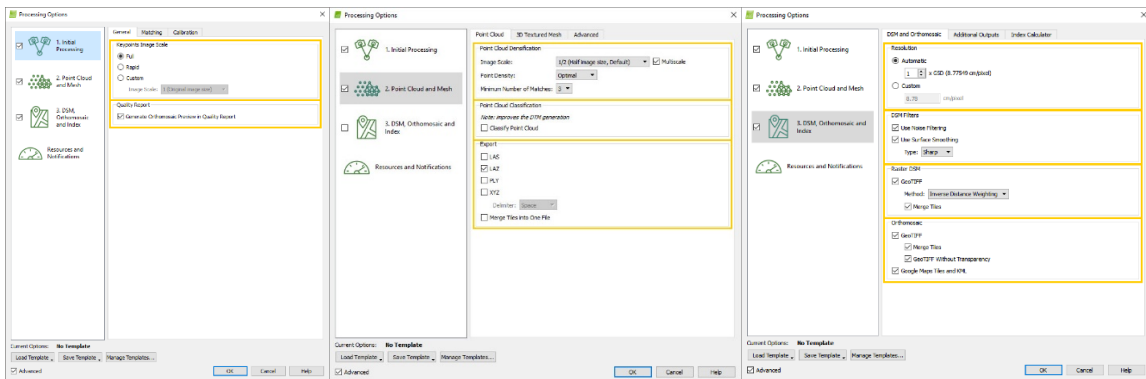


**Figure 19. Pix4D Processing Options**

Keypoints Image Scaling is the first processing option which allows the user to define the image size used to extract keypoints. For Keypoint Image Scaling there are three options: Full, Rapid, Custom. Full Scaling option set full Image Scale for more precise results and Rapid Scaling option set a lower Image Scale for less precise results and for faster results. Custom Scaling options includes double, half, quarter, eighth image scaling options and these options could be picked based on the users' needs. Next, Matching Image Pairs options can be used to select which pairs of images are matched. These options allow the users to optimize the image pairing process based on how the aerial images were captured. Based on how aerial images were captured, Aerial Grid or Corridor flight option and Free flight or Terrestrial options can be selected. Lastly, Image Calibration settings can be selected to set the number of keypoints extracted, how the camera internal and external parameters are optimized (using the Automatic Aerial Triangulation, Bundle Block Adjustment processes), to rematch image pairs for improving the quality of the reconstruction.

Point Cloud and Mesh Settings allow the users to change the scale of images that will be used to compute point cloud densification and additional 3D points. Point Cloud Classification settings can be selected to enable the generation of point cloud classification which generates Point Groups that are assigned with different classes such as Ground, Road Surface, High Vegetation, Building, and Human Made Object. Lastly, densified point cloud data can be exported in different output formats (.las, .laz, .ply, and .xyz) based on the user's selection. In the Mesh Settings, users can change the resolution and output quality of 3D textured mesh by selecting different resolution level parameters

(High, Medium, Low, Custom). 3D textured mesh can be exported as .ply, .fbx, .dxf, .obj, and u3d formats.

DSM/DTM and Orthomosaic Settings allow the users to set the spatial resolution of DSM and Orthomosaic files using automatic or custom ground sampling distance (GSD) value. In addition, DSM Filter options can be used to define parameters for noise filtering and surface smoothing the points of the point cloud data which are used to obtain the DSM. Raster DSM options can be used to set the method for the raster DSM generation. Inverse distance weighting algorithm (interpolate between points) and triangulation algorithm (Delauney triangulation) methods are available to users for selection. Former method is more suitable for buildings and latter method is more suitable for flat areas such as agriculture fields. Lastly, Orthomosaic Settings can be used to customize the output file format for the orthomosaic generation. Orthomosaic setting is set to save the orthomosaic image as a geotiff file by default.

Initially, Pix4D processing options were set to default and processed to generate digital surface model, digital terrain model, orthomosaic, point cloud, and 3D textured mesh. After the first data processing step, different processing option settings were selected. The second output data were compared with previous initial output data to examine the differences in quality of the data. data was preprocessed to reduce the overall processing time during photogrammetry processing and image processing steps. The main reason for preprocessing the data was to reduce noise and unnecessary objects in the images.

### **3.5 GIS Development**

First, an orthomosaic raster image of the test site was imported into ArcMap. The imported orthomosaic image included non-road features such as trees, sidewalks, and buildings. To clean non-road features from the orthomosaic image, raster clip operation was used. Roadways polygon shapefile obtained from Fairfax County GIS website was used to clip only road features on the orthomosaic image. This road orthomosaic clipping process before and after image can be seen in Figure 20.

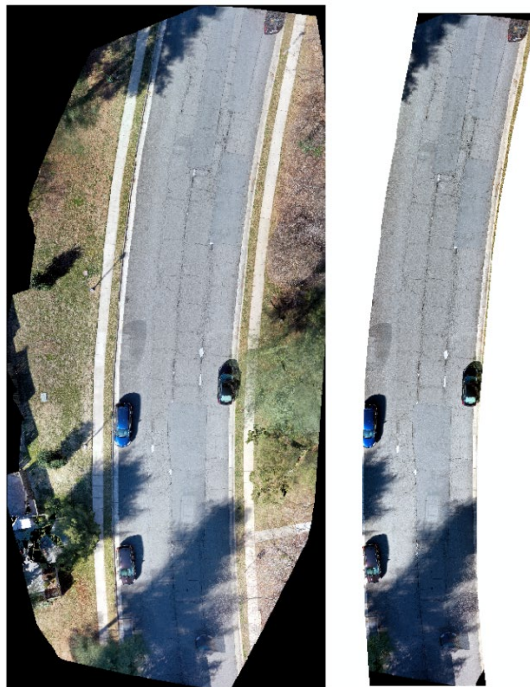


**Figure 20. Orthomosaic of Test Site Before and After Clip**

Next, roadways polygon shapefile was spatially joined with centerlines polygon shapefile to create road polygon shapefile with more attributes and feature identifiers

such as jurisdiction, postal code, road name and class, census feature class codes (CFCC). Roadways polygon and centerlines polygon data and attributes are displayed in Figure 21 below.

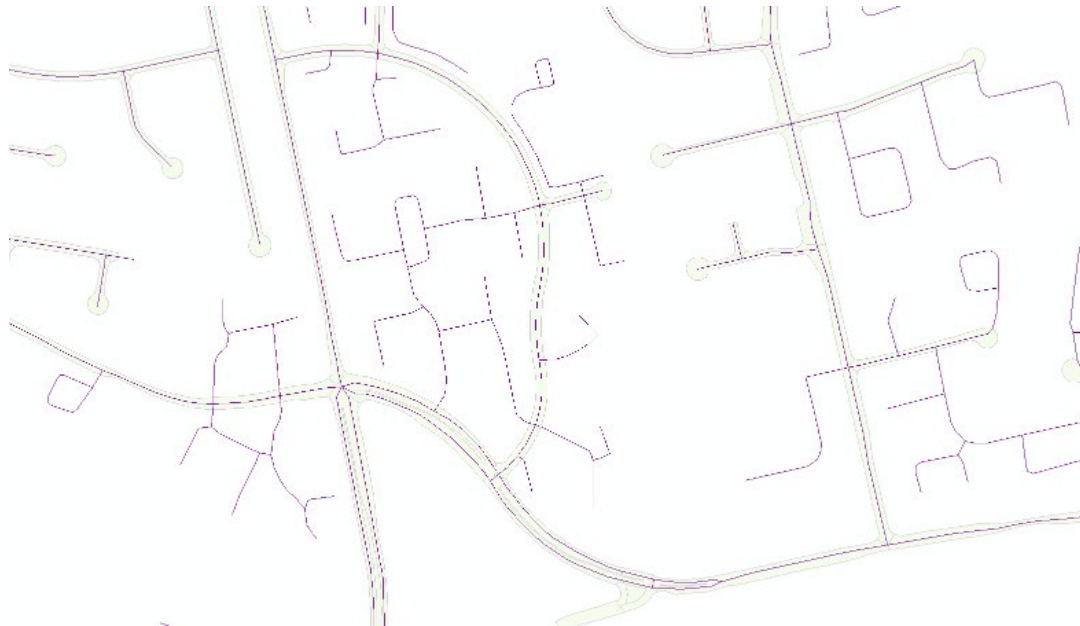


**Figure 21. Roadways and Centerlines Data**

For storing pothole data, a point feature class was created for input of known pothole metrics. i.e. x and y coordinates, pothole class type, length, width field. The points were manually added using the Editor Tool Pothole Class Type, Length, Width fields were manually added into the potholes attribute table. Class Type field was created using Short Integer datatype with Precision 0. Length, Width and Height fields were created using Double datatype with Precision: 9 and Scale5. The length and width sizes of potholes were then measured using the Measure tool in ArcMap and inserted in the

table. Based on the measured length and width sizes, potholes were then classified into three classes of severity: 1 – low severity, 2 – medium severity, 3 – high severity. The X and Y coordinates were automatically created in the attribute table using Add XY Coordinates tool from Data Management Toolbox. Next, Potholes shapefile was spatial joined with road polygon shapefile to produce more details and attributes in the pothole point shapefile. The final shapefile result of potholes data can be seen in Figure 22. Lastly, clipped road raster file was exported as tiff format with Rendered and Force RGB settings selected. This clipped road raster file was later used as an input image during the image processing step.



FID	Shape *	Class_Type	Length	Width	POINT_X	POINT_Y	TYPE	L_JURISDIC	L_POSTAL_A	FULLNAME	RW_TYPE_US	CFCC	ROAD_CLASS
0	Point	2	41.589	45.253	-77.300203	38.801514	Paved Road	FAIRFAX COUNTY	22032 (FAIRFAX)	COLONY VIEW DR	DRIVE (DR)	Local, neighborhood, and rural road, city street, unseparated	LOCAL ROAD
1	Point	1	0	0	-77.300226	38.801504	Paved Road	FAIRFAX COUNTY	22032 (FAIRFAX)	COLONY VIEW DR	DRIVE (DR)	Local, neighborhood, and rural road, city street, unseparated	LOCAL ROAD
2	Point	1	0	0	-77.30023	38.801477	Paved Road	FAIRFAX COUNTY	22032 (FAIRFAX)	COLONY VIEW DR	DRIVE (DR)	Local, neighborhood, and rural road, city street, unseparated	LOCAL ROAD
3	Point	1	0	0	-77.30024	38.801379	Paved Road	FAIRFAX COUNTY	22032 (FAIRFAX)	COLONY VIEW DR	DRIVE (DR)	Local, neighborhood, and rural road, city street, unseparated	LOCAL ROAD
4	Point	2	0	0	-77.300207	38.801346	Paved Road	FAIRFAX COUNTY	22032 (FAIRFAX)	COLONY VIEW DR	DRIVE (DR)	Local, neighborhood, and rural road, city street, unseparated	LOCAL ROAD
5	Point	2	0	0	-77.300243	38.801312	Paved Road	FAIRFAX COUNTY	22032 (FAIRFAX)	COLONY VIEW DR	DRIVE (DR)	Local, neighborhood, and rural road, city street, unseparated	LOCAL ROAD
6	Point	2	0	0	-77.300269	38.801251	Paved Road	FAIRFAX COUNTY	22032 (FAIRFAX)	COLONY VIEW DR	DRIVE (DR)	Local, neighborhood, and rural road, city street, unseparated	LOCAL ROAD
7	Point	1	0	0	-77.300243	38.801198	Paved Road	FAIRFAX COUNTY	22032 (FAIRFAX)	COLONY VIEW DR	DRIVE (DR)	Local, neighborhood, and rural road, city street, unseparated	LOCAL ROAD
8	Point	1	0	0	-77.300241	38.801673	Paved Road	FAIRFAX COUNTY	22032 (FAIRFAX)	COLONY VIEW DR	DRIVE (DR)	Local, neighborhood, and rural road, city street, unseparated	LOCAL ROAD
9	Point	1	0	0	-77.300182	38.80155	Paved Road	FAIRFAX COUNTY	22032 (FAIRFAX)	COLONY VIEW DR	DRIVE (DR)	Local, neighborhood, and rural road, city street, unseparated	LOCAL ROAD

Figure 22. Example of Pothole Shapefile Data

Manually inputting length/width sizes and identifying potholes may not be a time-efficient method to use for creating large georeferenced datasets of potholes. However, for most local transportation authorities, pothole patching repairs are done at a small segmented road-scale level. Therefore, it would be more time efficient and safer for road repair crews to conduct quick in situ surveys using UAVs and collect potential pothole data rather than driving traditional road vehicles and being constrained to the traffic flow

and speed. Although manual input of pothole data is time-consuming, municipal road repair crews can expand upon the pothole data record which will provide not only backlogs of unrepaired potholes, but also determine which potholes need to be repaired first based on the level of severity. This method and the output pothole data produced much higher quality and locational accuracy of both known and unknown potholes on the roads than existing pothole data from Washington D.C. GIS dataset, which only had about 45% location accuracy of the potholes.

### **3.6 3D Reconstruction**

3D reconstruction step used previously processed .las point cloud data from Pix4Dmapper. During 3D reconstruction step, CloudCompare, an open source 3D point cloud and mesh processing software, Autodesk Recap Pro, and Civil 3D was used. Initially, CloudCompare was used to import .las point cloud data file. After importing the point cloud data, potential pothole areas were segmented using Segment Tool and by drawing ROI around the potential potholes. This process can be seen in Figure 23.



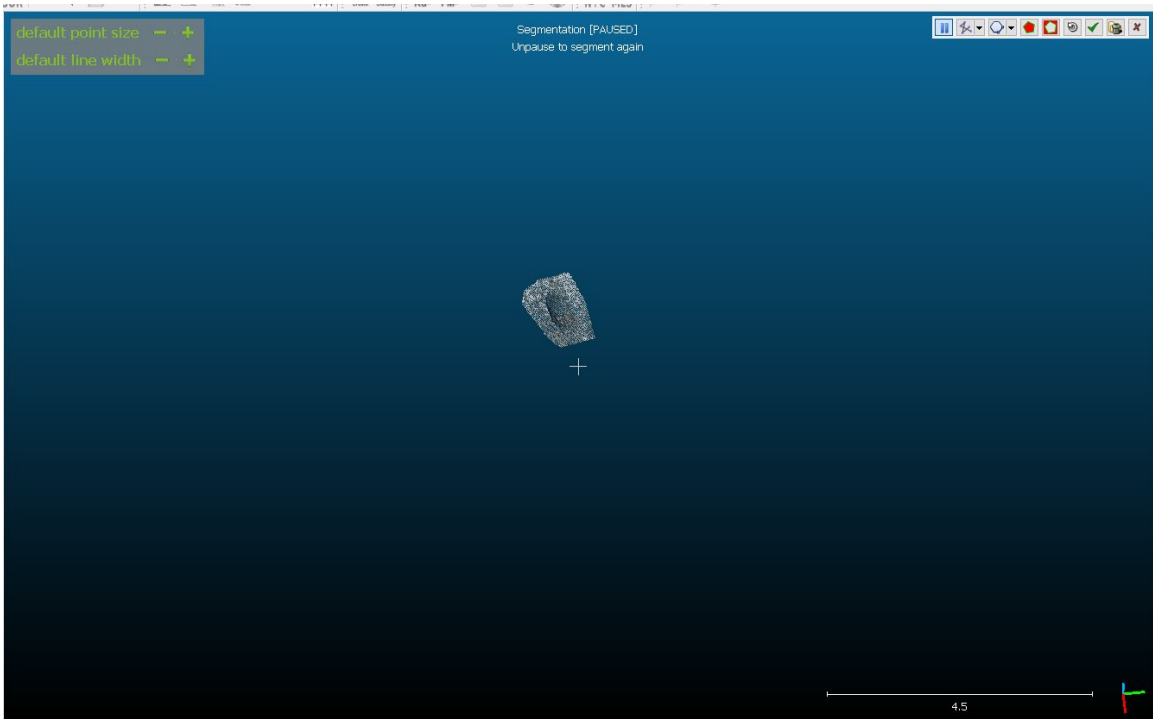


**Figure 23. Importing, Segmenting and Clipping Point Cloud**

Potential pothole area(s) was segmented out of other point cloud data. After the segmentation process, the SOR (Statistical Outlier Removal) tool was used to compute the first average distance of each point to its neighbors – considering  $k$  nearest neighbors for each –  $k$  is the first parameter. This removes points that are farther than the average distance plus a number of times the standard deviation which is the second parameter of this tool (Figure 24).

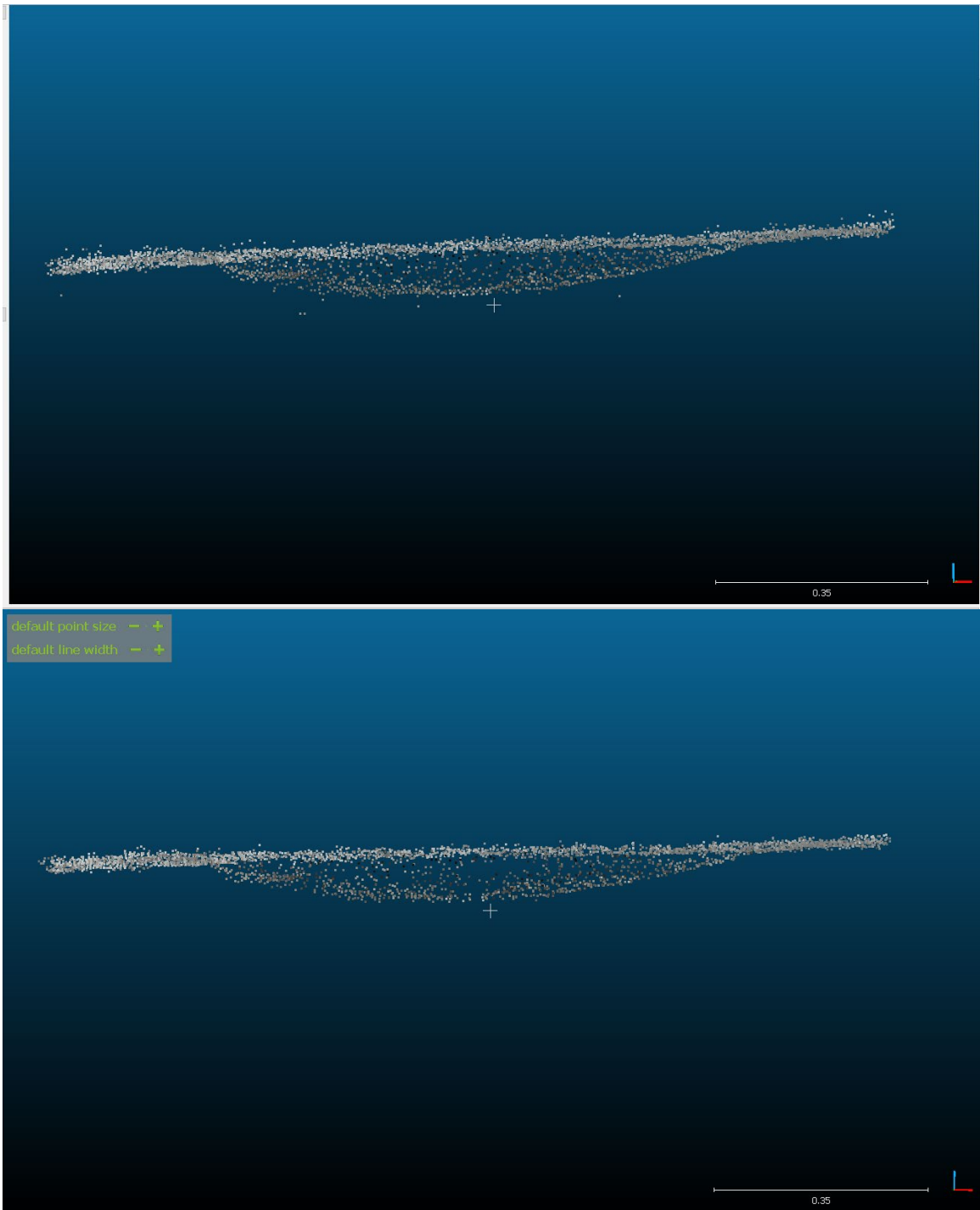


**Figure 24. Before and After Noise Removal of Point Cloud Data**

Once the segmented point cloud data were cleaned up, Compute 2.5D Volume Tool was used to validate relative elevation/height difference that helped determine if there was a pothole in the segmented point cloud area (Figure 25). After validating the pothole in the point cloud data, the segmented point cloud data was exported as a .las format file.

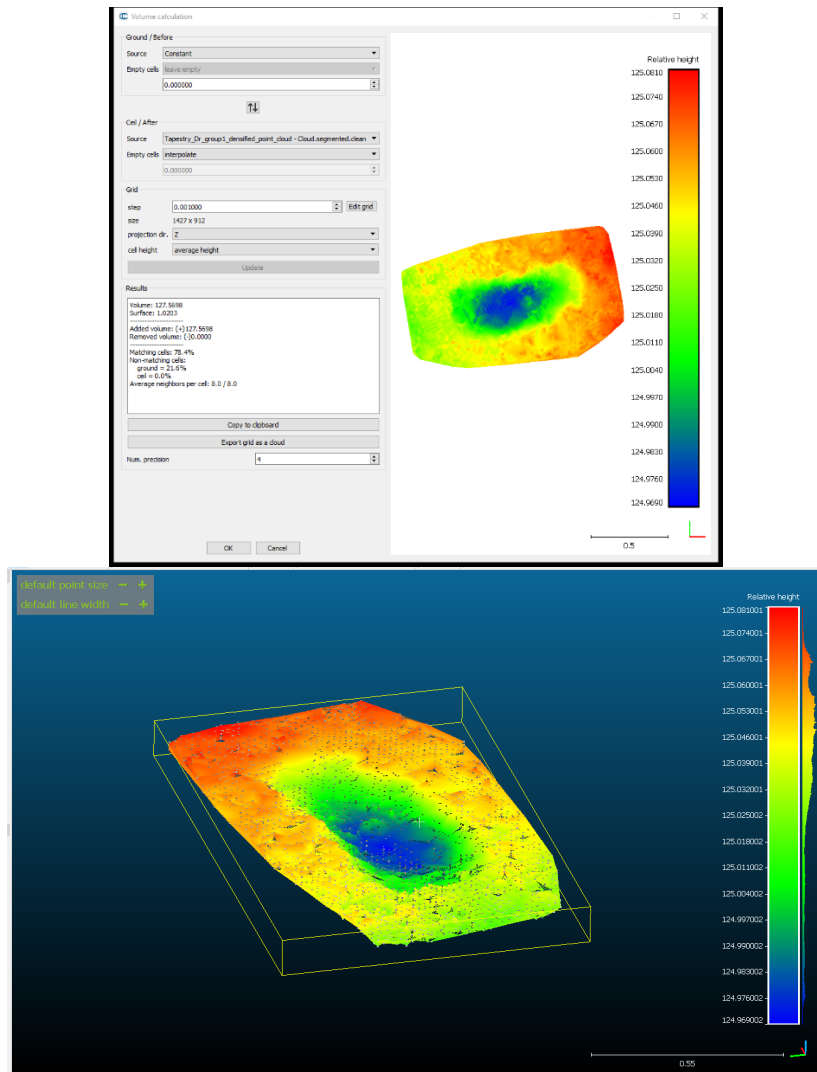


Figure 25. 2.5D Volume Measurement and Point Cloud

After using CloudCompare to segment, filter, and validate pothole point cloud data, the output .las file was imported in Recap Pro. Recap Pro was only used to convert .las file to .res format which can be used in Autodesk's AutoCAD software. Imported .res format point cloud data in AutoCAD Civil 3D can be seen in Figure 26.

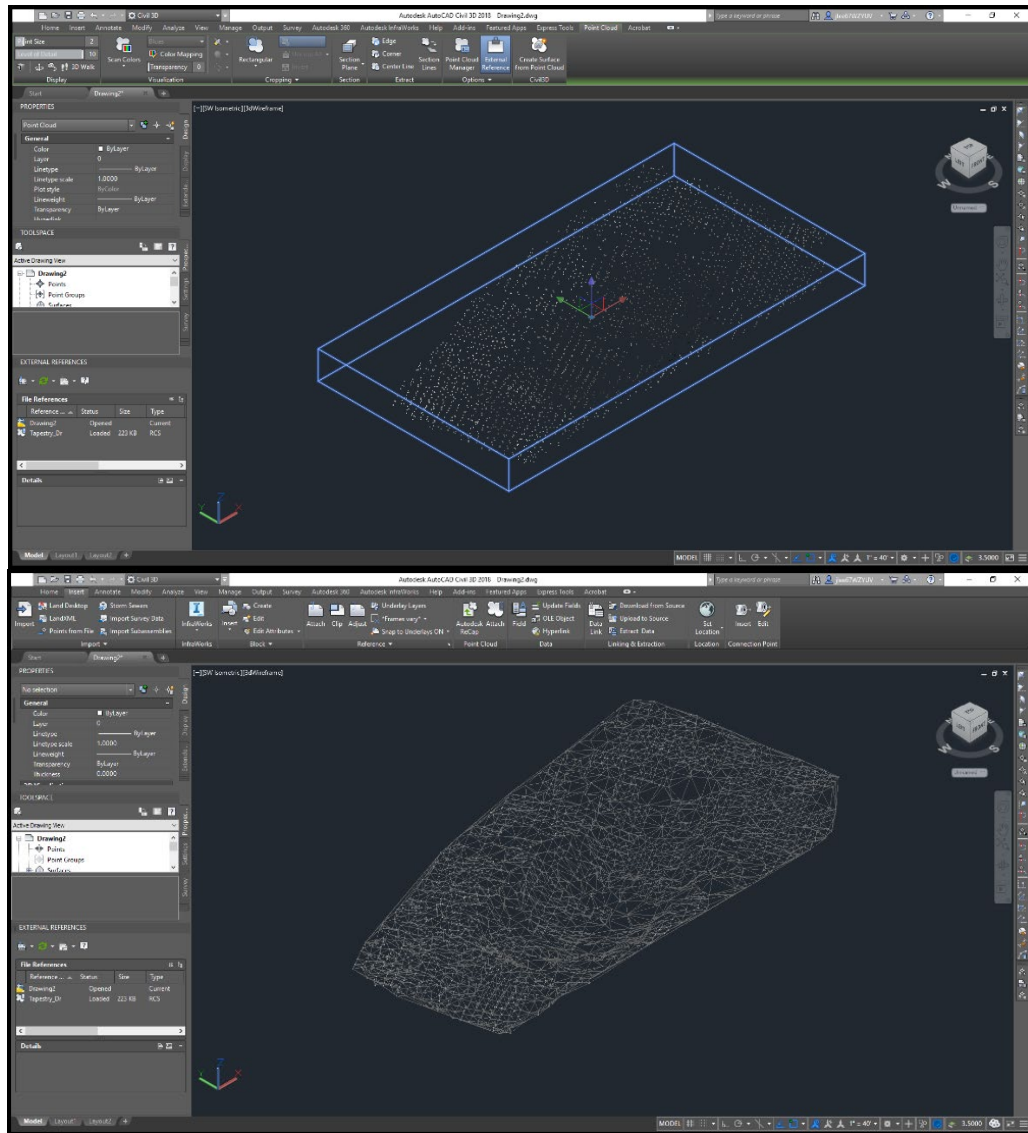


Figure 26. AutoCAD Civil 3D Point Cloud Display and TIN Surface

After the conversion process, Civil 3D was used to calculate/estimate the pothole volume from .rcs point cloud data. Since the point cloud data was not georeferenced, when the .rcs file was imported a coordinate system had to be added to the workspace (Figure 27).

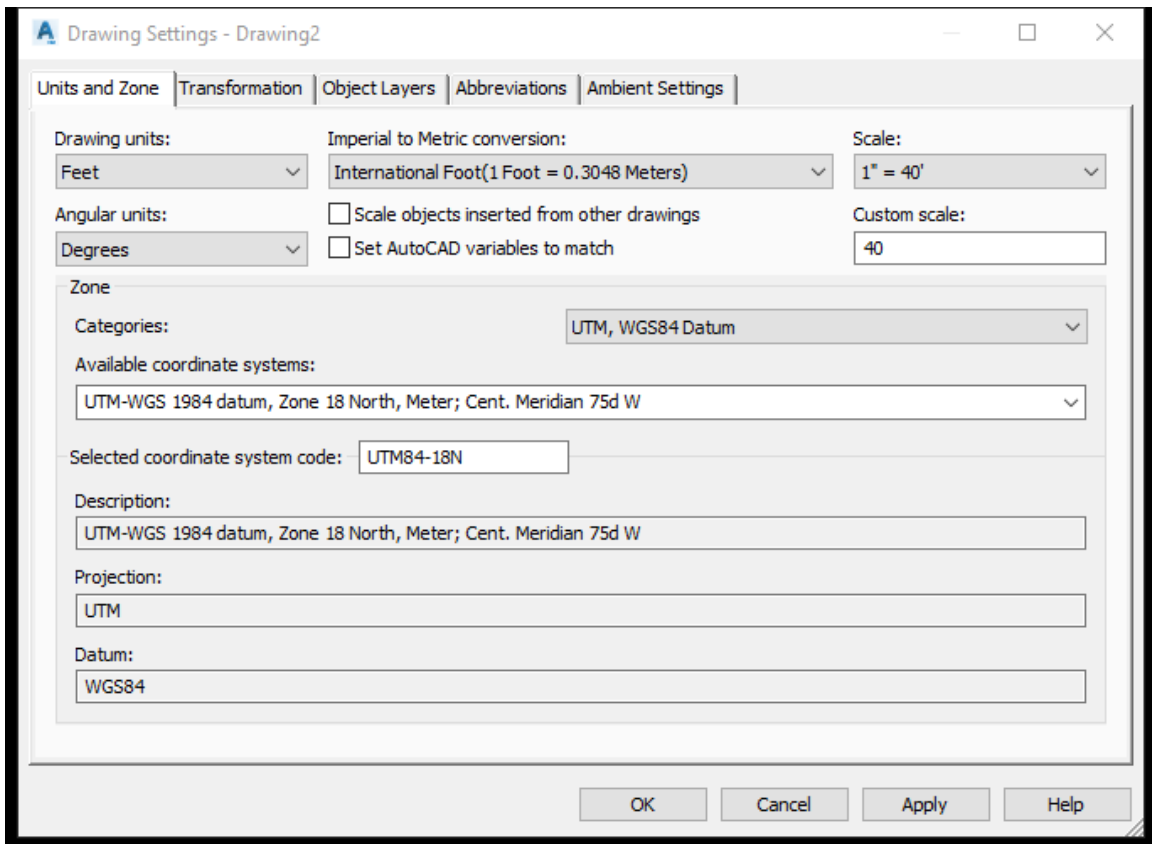


Figure 27. Georeferencing Point Cloud in Civil 3D

Next, a TIN surface was generated using the point cloud data with Kriging Interpolation filter method setting enabled. Kriging interpolation filter method was used

to interpolate data points to build more curves. Using this TIN surface, a borderline of the TIN surface layer was extracted (Figure 28).

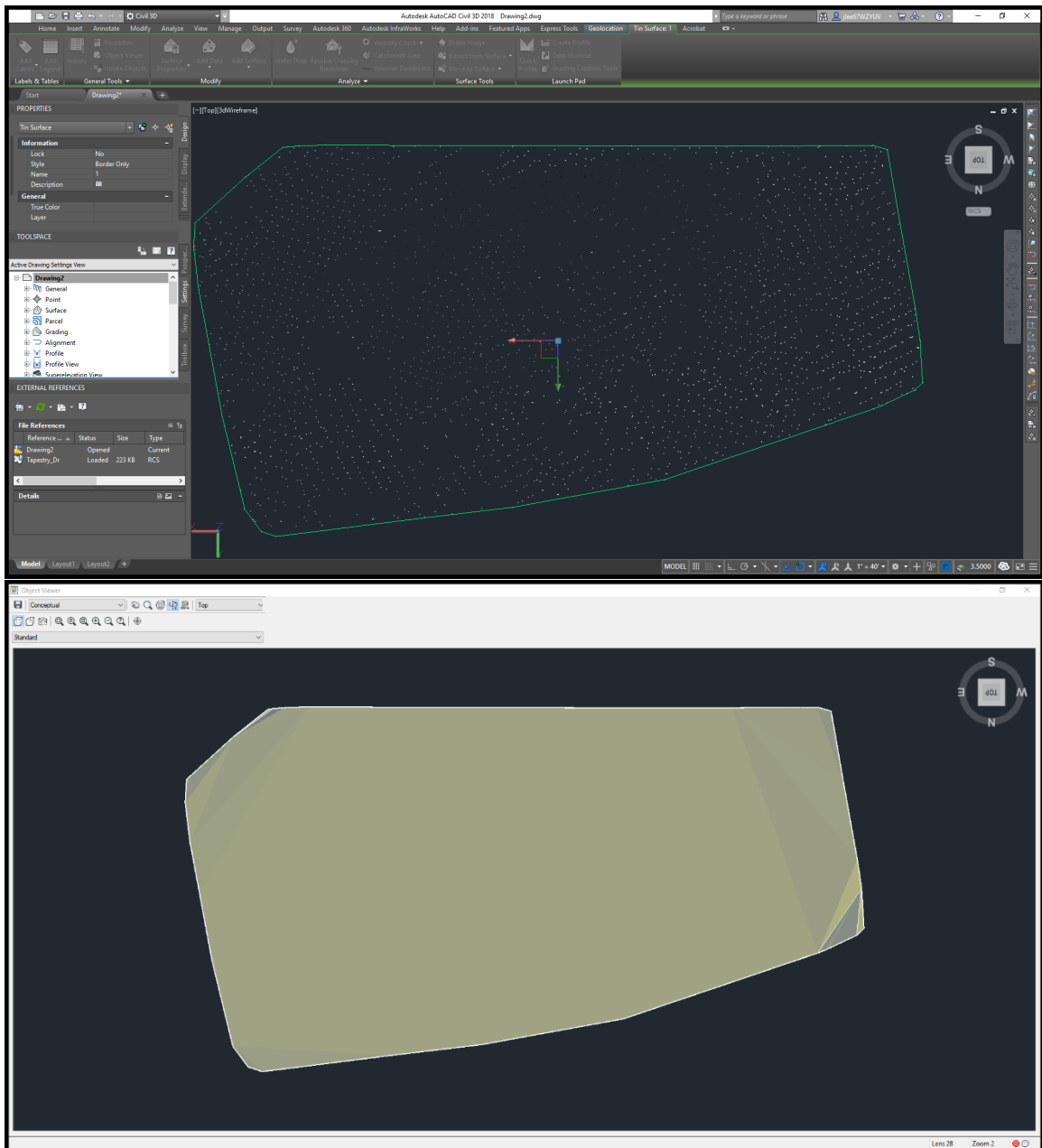
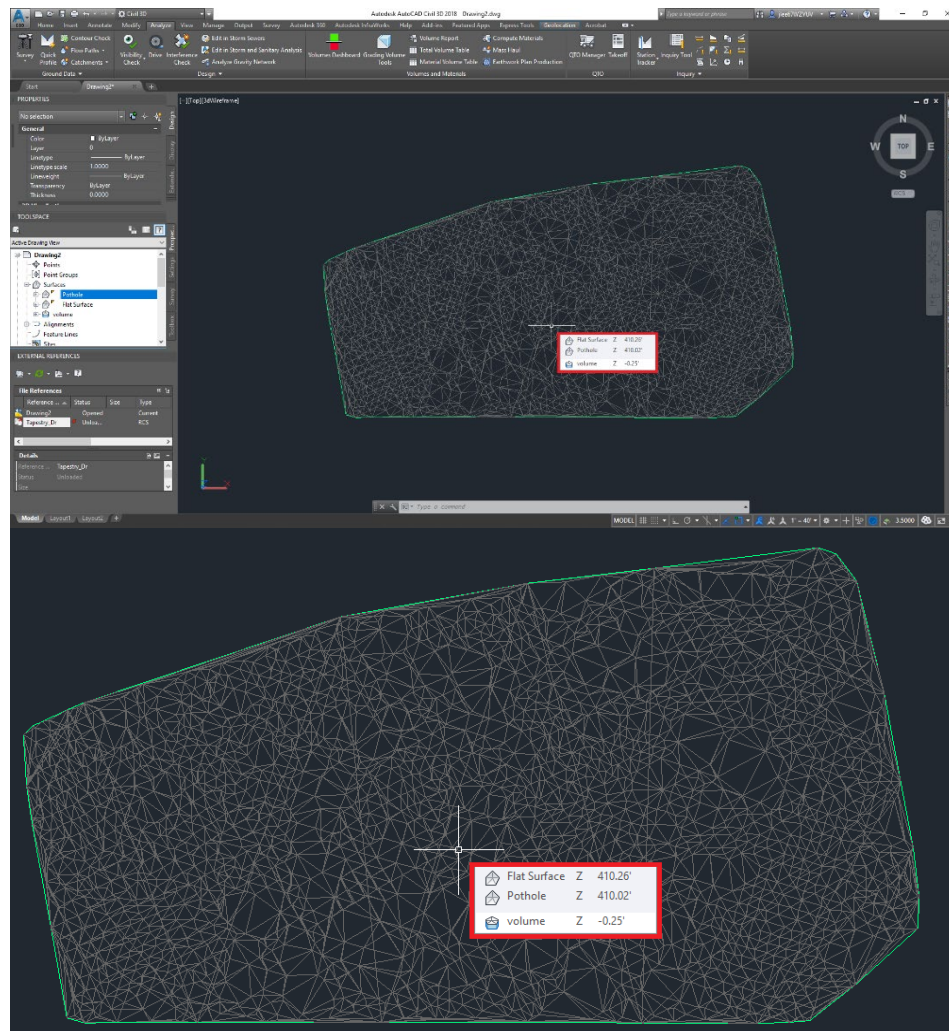


Figure 28. Borderline - Base 3D Surface Model

The extracted borderline generated a flat, base TIN surface layer. Two TIN surface layers: pothole TIN surface layer and base TIN surface layer was used to generate a TIN volume surface. Finally, pothole TIN surface layer and base TIN surface layer was used to calculate the elevation (Z-value) of the TIN volume surface layer. This calculated Z-value was used as an estimate of elevation of the pothole depth. This the output of this process is depicted in Figure 29. After acquiring the Z-values of the pothole point cloud data, Z-values were compared to the ground truth height measurement to test the accuracy of this 3D reconstruction method.



**Figure 29. Z-value Estimation Surface Height - Pothole Depth**

### **3.7 Image Processing Detection**

To test the feasibility of image processing detection of potholes, Marker-Controlled Watershed Segmentation method was used. This method was used to separate touching objects in the aerial image. Previously clipped road raster file was used as input image file in MATLAB. MATLAB is used for image processing detection steps because MATLAB offers a wide variety of tools that can perform image segmentation, filtering

and enhancement, and object detection and analysis out of the box. First, the input image was converted to grayscale image. Grayscale image was used to compute the gradient magnitude which indicated the borders of the objects. This gradient magnitude was used as a segmentation function (Figure 30). To compute the gradient magnitude, Sobel gradient operator method was used by default.

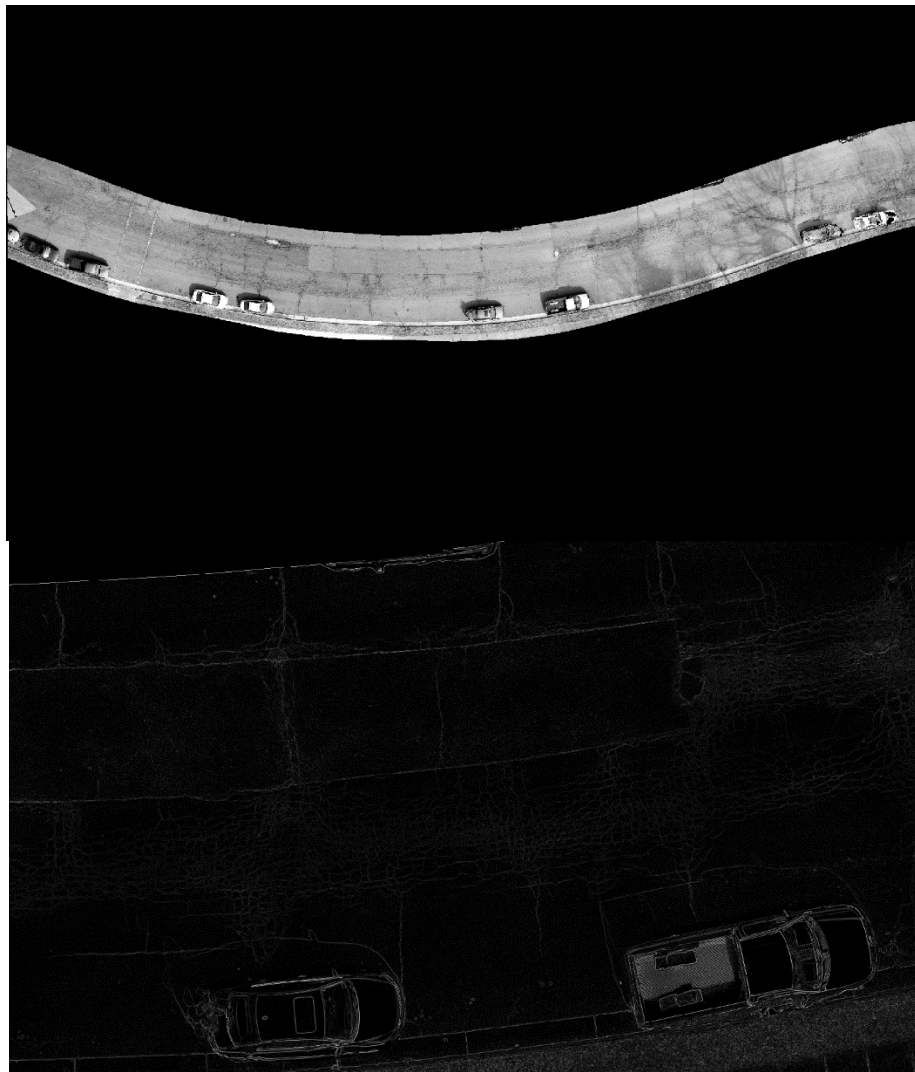


**Figure 30. Grayscale Converted and Computed Gradient Magnitude**

After computing this segmentation function, foreground objects had to be marked. To mark the foreground objects morphological techniques: erosion and dilation was used for reconstruction-based opening-closing process. Next, background markers were computed by using a thresholding operation and separated the background pixels which were not part of any object. The gradient magnitude was modified to have regional minima only in certain desired locations so that the gradient magnitude image, which is the segmentation function, its regional minima occur at the foreground and background marker pixels. Finally, watershed-based segmentation was performed. The result is depicted in Figure 31.



**Figure 31. Watershed-based Segmentation Sample Result**

## CHAPTER FOUR: RESULTS

This chapter of thesis summarizes the results from the project working demonstration performed at different pilot study test sites outlined in 3.3 Pilot Study section. Each following section reviews the input and results from each stage of the workflow.

### 4.1 Pilot Study 1

The first pilot study site was Tapestry Drive, Fairfax, Virginia (Figure 32).

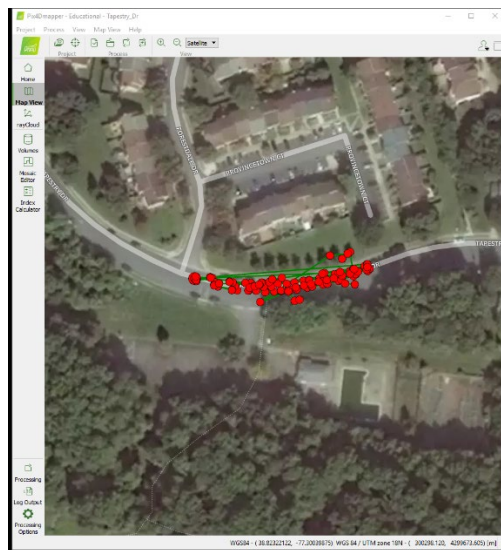


Figure 32. Pilot Study Site 1: Tapestry Drive

The first aerial survey was conducted at 20m altitude. However, due to the height of surrounding trees, the altitude had to be adjusted to 25m to ensure the safety of the drone and the flight mission. During this first pilot study, 110 images were captured. For this pilot study, the first flight captured images at 80% overlap and in nadir view. The second flight captured images at 45° obtain higher height spatial resolution of the roads. The grid pattern was used for this pilot study's route design. The camera angles and overlaps in Figure 33.

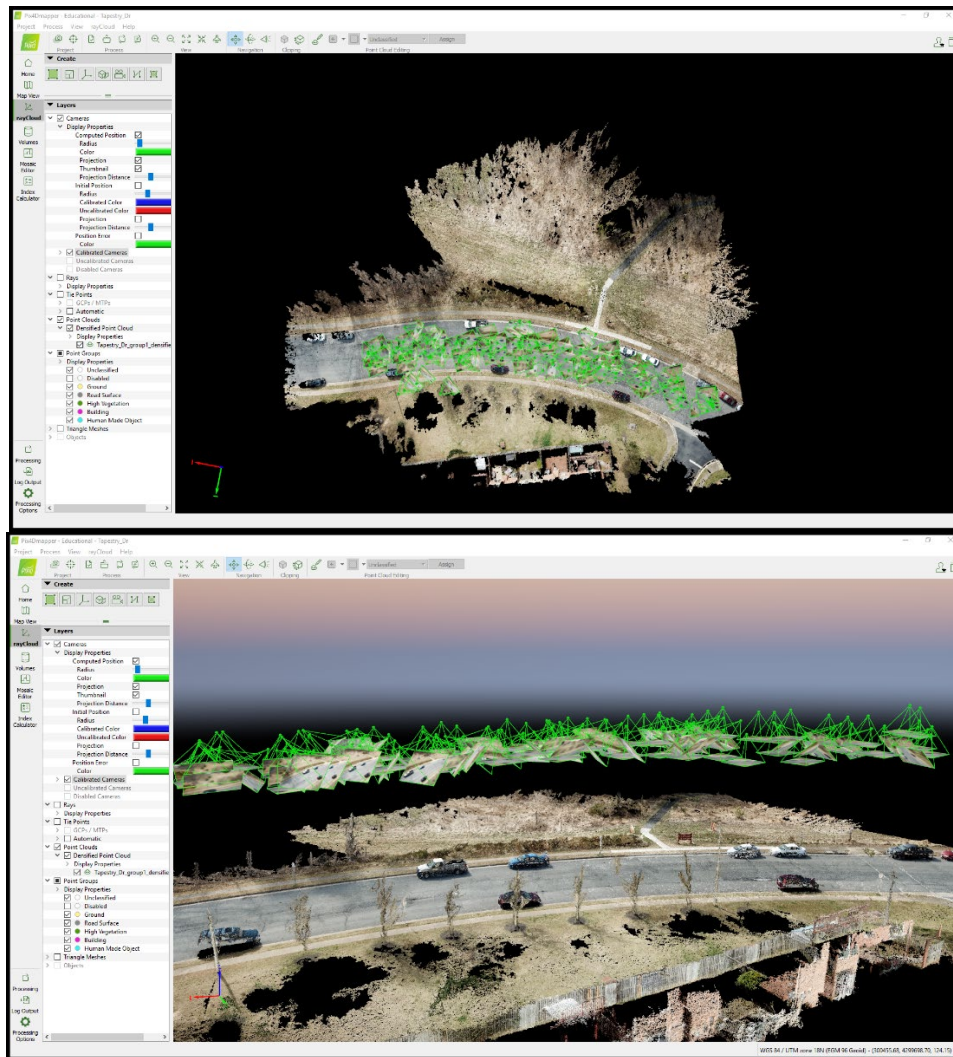


Figure 33. Tapestry Drive: Point Cloud and Camera Setup – Top and Side View

The ground truth measurement of the potholes can be found in Table 4 below. In addition, the reference map with pothole sample number labels can be seen in Figure 34.

Table 4. Pilot Study 1 Ground Truth Measurement

Sample #	Length	Width	Height
1	36.4 inches	15.5 inches	2.7 inches
2	19.8 inches	12.5 inches	1.4 inches
3	12.6 inches	3.1 inches	1.3 inches

The ground truth measurement data were used to test the accuracy during the GIS development step process and can be found in Table 5.



**Figure 34. Tapestry Drive: Annotated Potholes**

Once images have been collected, these images were then transferred and uploaded to Pix4Dmapper. Based on Pix4Dmapper calculations, the average ground sampling distance was 0.64 cm and 1.7657 acres of land were covered. The median number of keypoints per image was 33,659 keypoints. All of 110 images that were captured were calibrated. The median number of matched keypoints was 14,987 matches per calibrated image. An orthomosaic and the corresponding sparse digital surface model can be seen below.

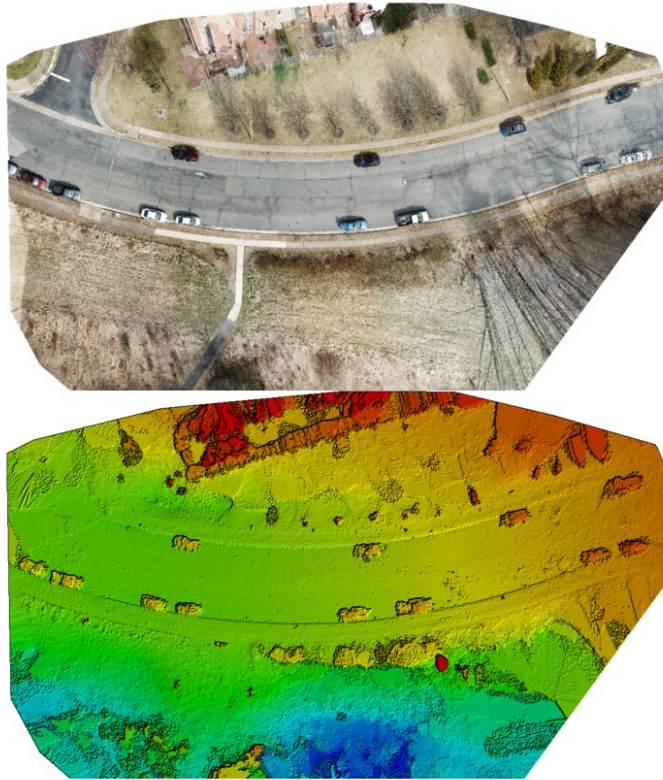
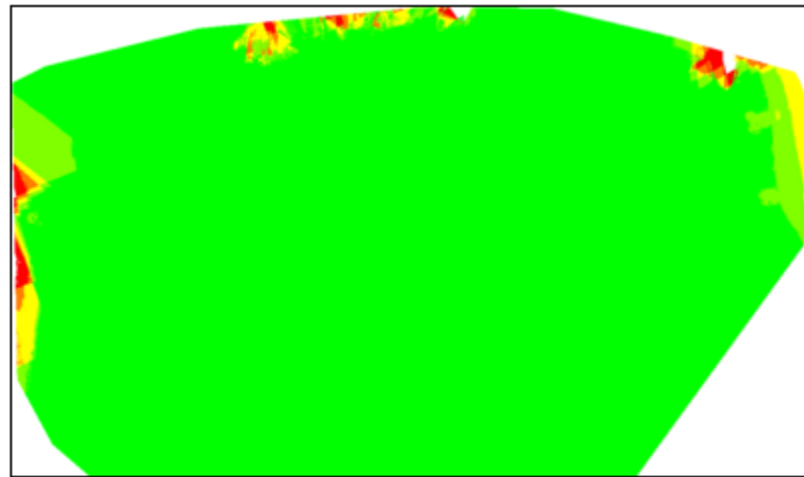


**Figure 35. Tapestry Drive: Orthomosaic and DSM**

In addition, the overlap images can be seen in Figure 36. This figure depicts the number of overlapping images that were computed for each pixel of the orthomosaic. Red to Yellow areas indicated low overlap which resulted in poor results and green areas included overlap of over five images for every pixel.



Number of overlapping images: 1 2 3 4 5+  
**Figure 36. Tapestry Drive: Overlapping Images for the Orthomosaic**

Time for point cloud densification was approximately 10 minutes, time for point cloud classification was approximately 21 seconds. Time for 3D textured mesh generation was 3 minutes 12 seconds. The number of 3D densified points was 8,132,336 points and the average density per cubic meter was 7,751.94 points. The digital surface model and orthomosaic resolution was 0.637 cm/pixel. Time for DSM generation was 7 minutes 11 seconds and time for orthomosaic generation was 13 minutes 51 seconds. Overall, processing point cloud densification, classification, textured mesh generation, to DSM and orthomosaic generation took approximately 35 minutes. The Pix4D point cloud output can be seen in Figure 33.

The result of GIS development was a file geodatabase that contains a pothole shapefile with x, y, z coordinates of the potential potholes, length, width, height, and other attributes such as road names, jurisdiction, postal code, and road class. This

geodatabase also included an orthomosaic road clipped image. The attribute table of the potholes and the clipped road image can be seen in Figure 37 below.



Figure 37. Tapestry Drive: Clipped Road and Pothole Data

After potential potholes have been manually identified during GIS development, the point cloud data was imported into CloudCompare, a photogrammetry processing software (Figure 38).

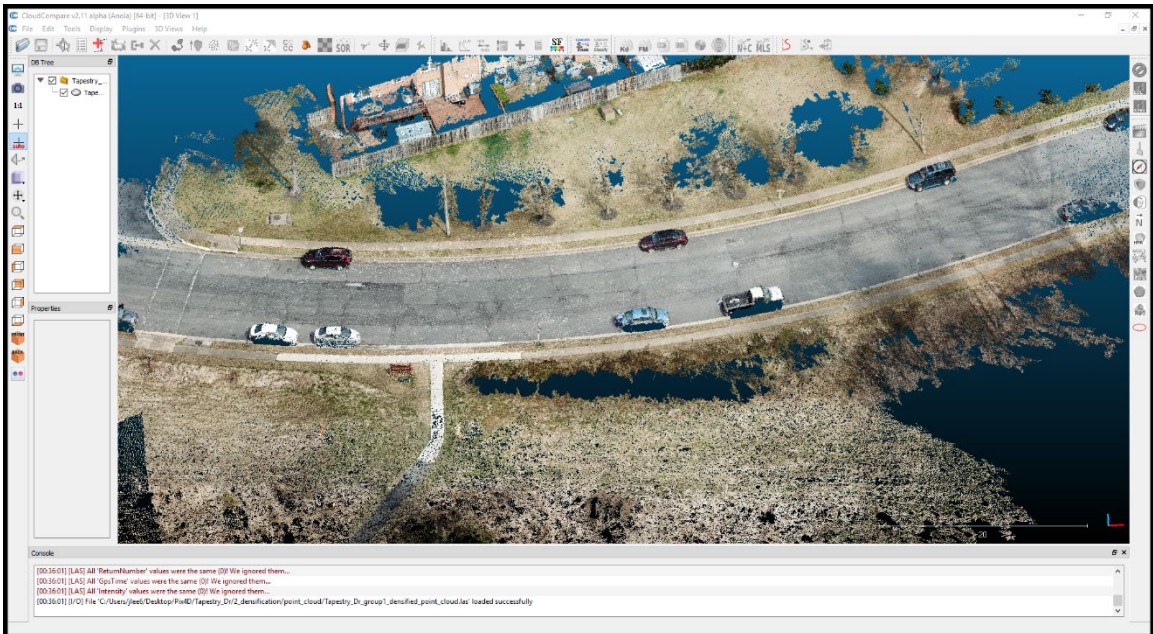


**Figure 38. Tapestry Drive: Point Cloud**

Total of three potential potholes have been extracted. Three potential potholes have been clipped, extracted and segmented from the rest of the point cloud (Figure 39).

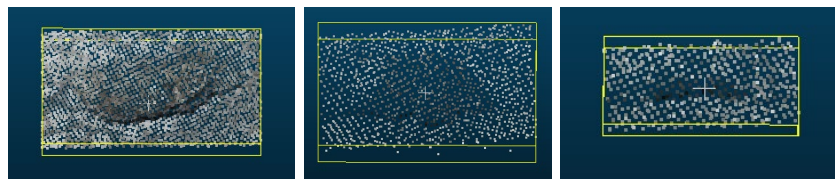


**Figure 39. Clipped Point Cloud: Sample 1, 2, 3**

Each sample have been applied with the Statistical Outlier Removal (SOR) filter. The first, second, and third sample (side-view) before and after filter can be seen in Figure 40, respectively. Sample 1 contained 3,343 points before the filter was applied and had 2,889 points after the filter. Sample 2 contained 1,439 points before the filter was

applied and had 1,346 points after the filter. Sample 3 contained 605 points and had 534 points after the filter. These filtered sample point clouds were exported as .las files and used as input in Autodesk ReCap Pro for conversion.

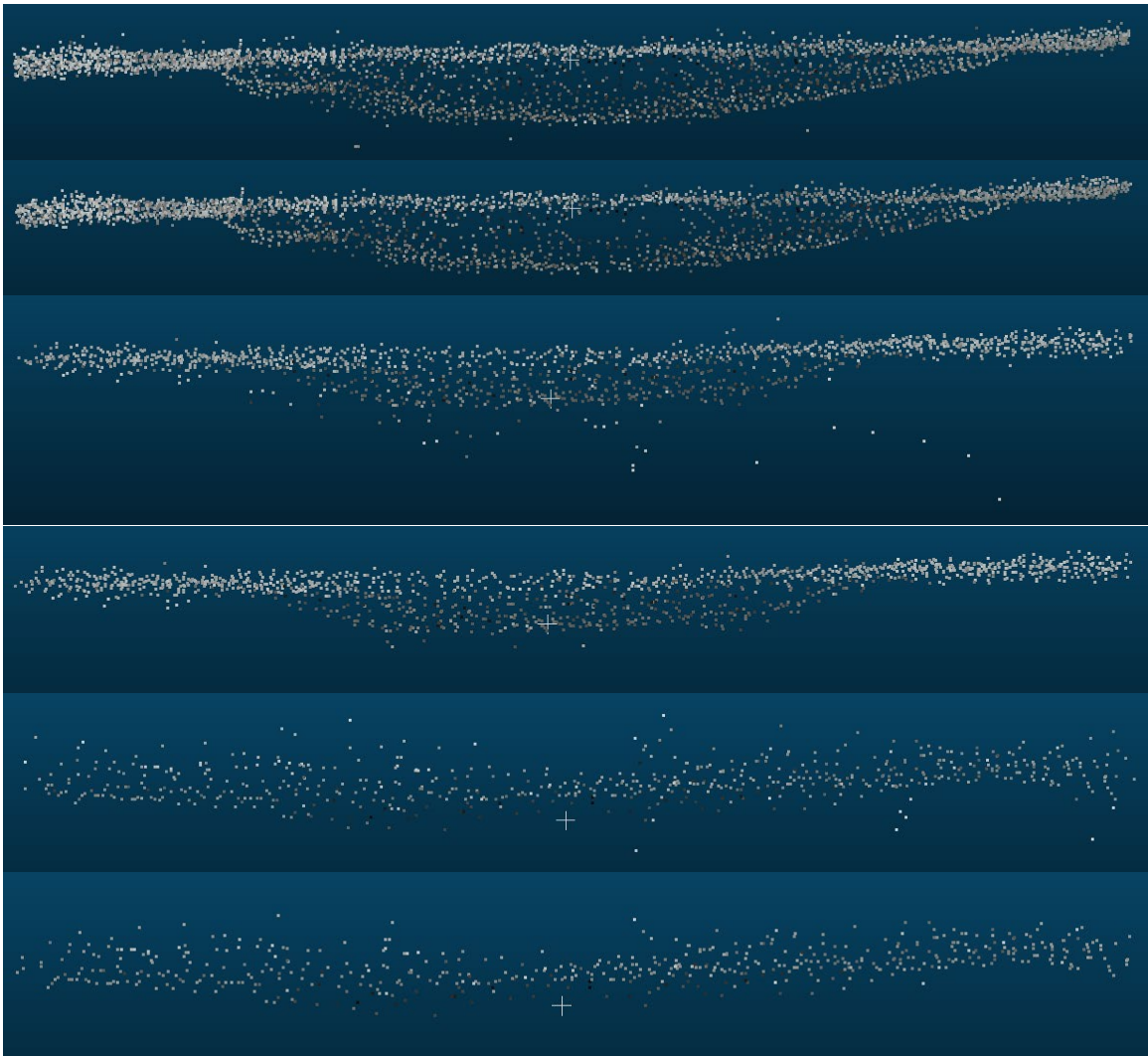


**Figure 40. Sample 1, 2, 3 Side View Before and After Filter**

Once the .las data was converted to .rcs data, .rcs was loaded into Autocad Civil 3D for measuring the depth of the potholes. Figure 41 depicts the loaded point cloud in Autocad Civil 3D software. Pothole height was calculated using z-value differences between the flat surface and the potholes.

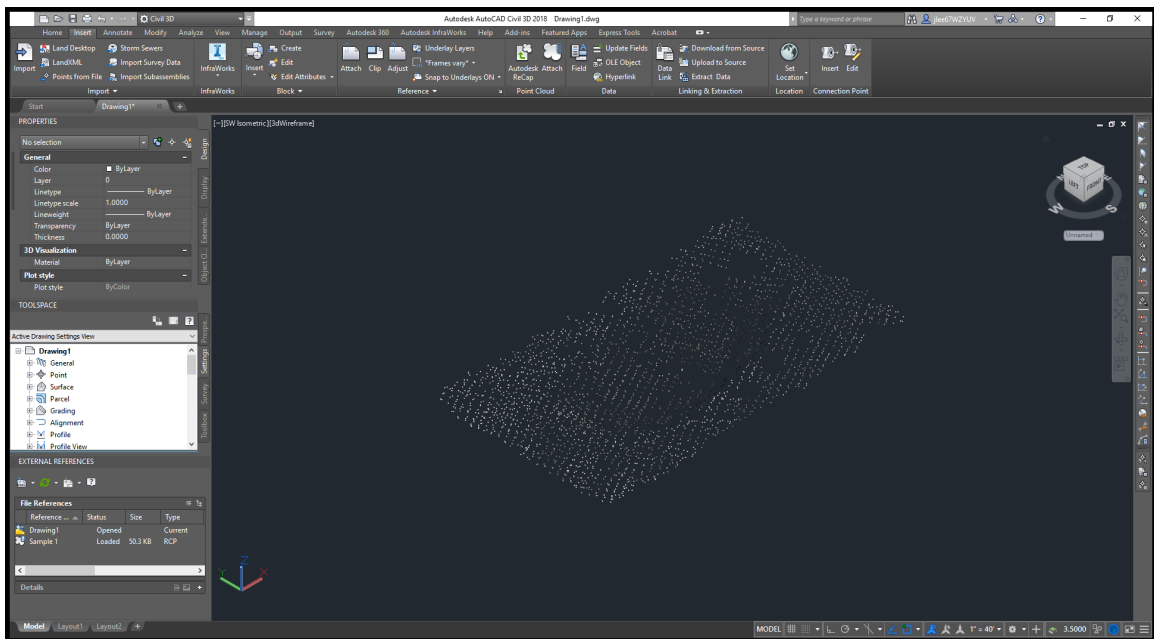


Figure 41. Sample 1 Point Cloud in Civil 3D

TIN surface was created using the Sample 1 point cloud and Kriging interpolation method. Kriging interpolation was used to filter out non-ground points and to build smoother TIN surface. Figure 42 depicts the Sample 1 TIN surface layer.

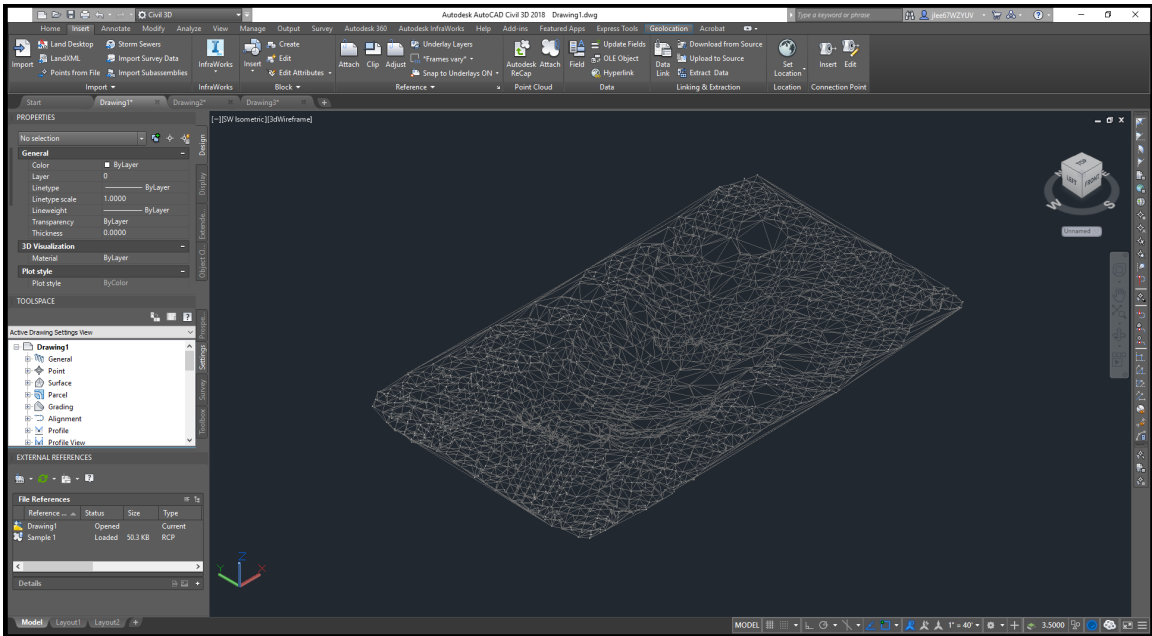
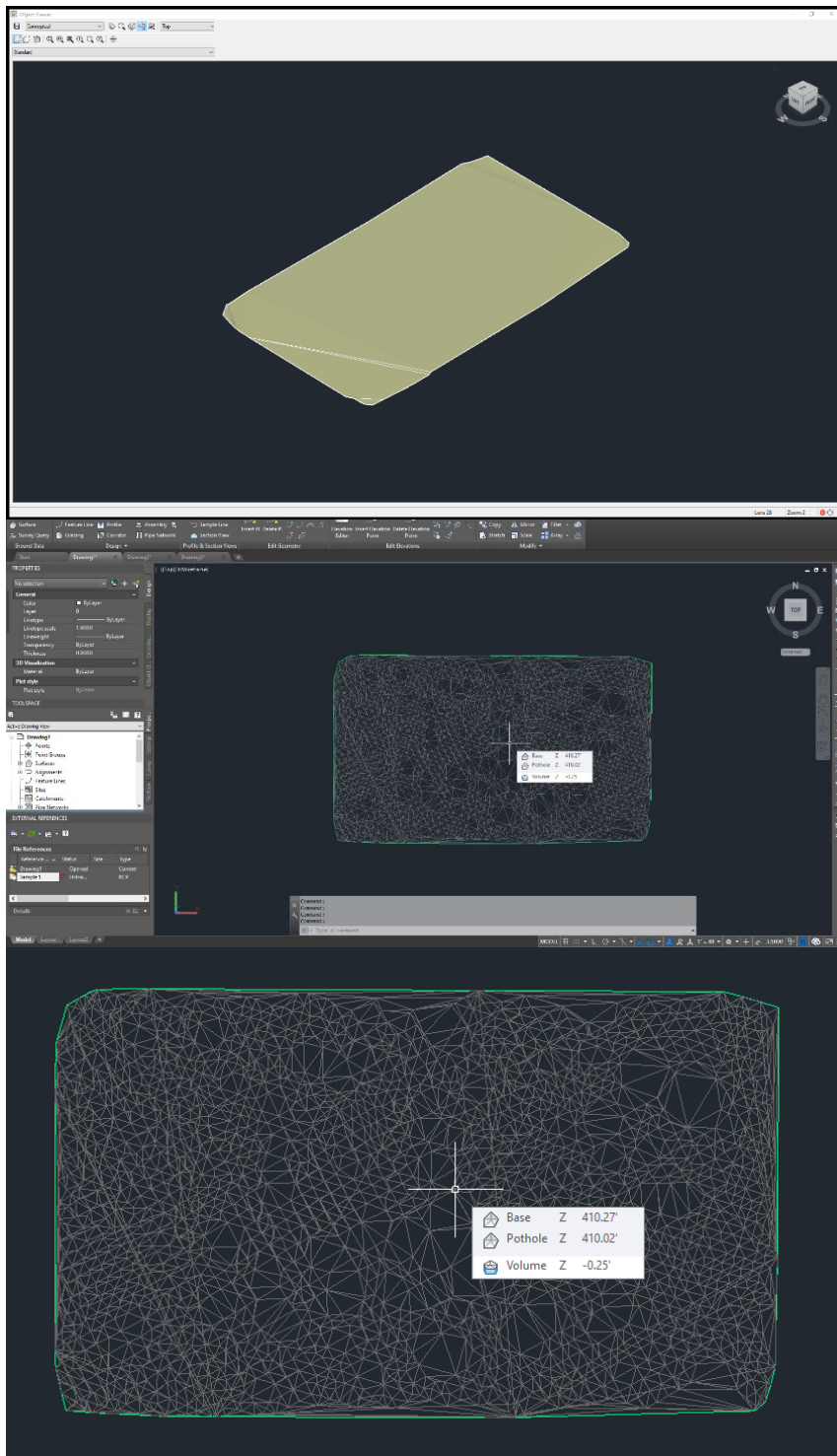


Figure 42. Sample 1 TIN Surface Layer

Using the TIN surface, a surface layer was created using the boundary of the Sample 1 TIN surface layer. This flat base surface layer was used to calculate the height difference between the bottom of the pothole TIN surface layer and the top height of the base surface layer. The flat base surface layer, pothole TIN surface layer and the calculated Z-value can be seen in Figure 43.



**Figure 43. Sample 1 Base Surface and Pothole Surface Z-values**

Sample 2 and Sample 3 results are depicted in Figure 44. The z-values of each pothole for Pilot Study 1 are listed in Table 5 below.

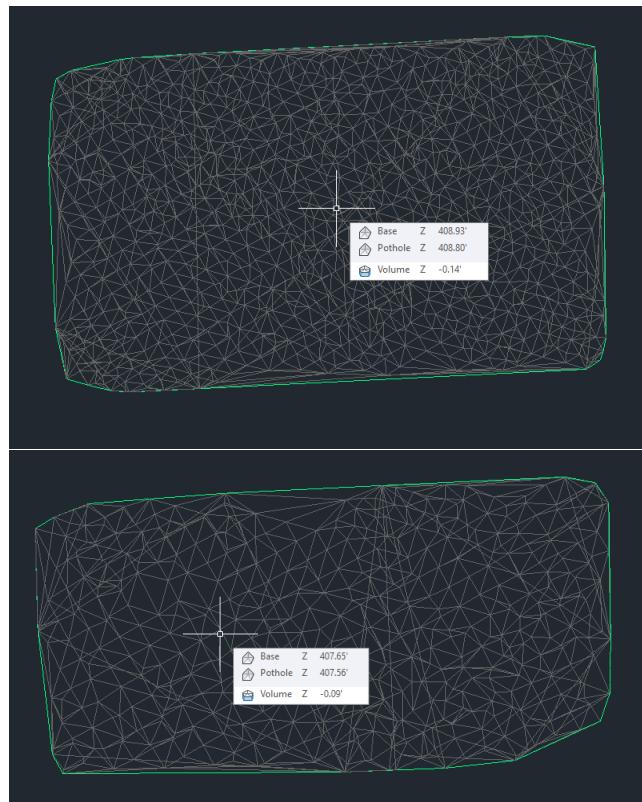


**Figure 44. Sample 2 and 3 Z-values**

After collecting the height information from 3D reconstruction step, Z-value or height value can be included in the aforementioned GIS pothole dataset. The size accuracy of the potholes can be calculated using the ground truth measurement data and the GIS and 3D reconstruction measured data.

**Table 5. Pilot Study 1 Identified Measurement**

<b>Sample #</b>	<b>Length</b>	<b>Width</b>	<b>Height</b>
1	36.8 inches	15.3 inches	2.5 inches
2	20.8 inches	12.8 inches	1.4 inches
3	12.35 inches	3.1 inches	0.9 inches

Based on the ground truth measurement data and the identified measured data of Sample 1, absolute accuracy values of the identified measurement are depicted in Table 6.

**Table 6. Pilot Study 1 Identified Measurement Accuracy**

<b>Sample #</b>	<b>Length</b>	<b>Width</b>	<b>Height</b>
1	+0.4 inches	-0.2 inches	-0.2 inches
2	+1.0 inches	+0.3 inches	0 inches
3	-0.25 inches	0 inches	-0.4 inches

Length measurement: +0.4 inches, width measurement: -0.2 inches, and height measurement: -0.2 inches. Sample 2 length measurement: +1.0 inches, width: +0.3 inches, and height: 0 inches. Sample 3 length measurement: -0.25 inches, width: 0 inches, and height: -0.4 inches. The results of Pilot Study 1 were promising since the identified measurement value had an absolute accuracy of +/- 1.0 inch.

#### **4.2 Pilot Study 2**

The second pilot study was conducted on Colony View Drive, Fairfax, Virginia (Figure 45).

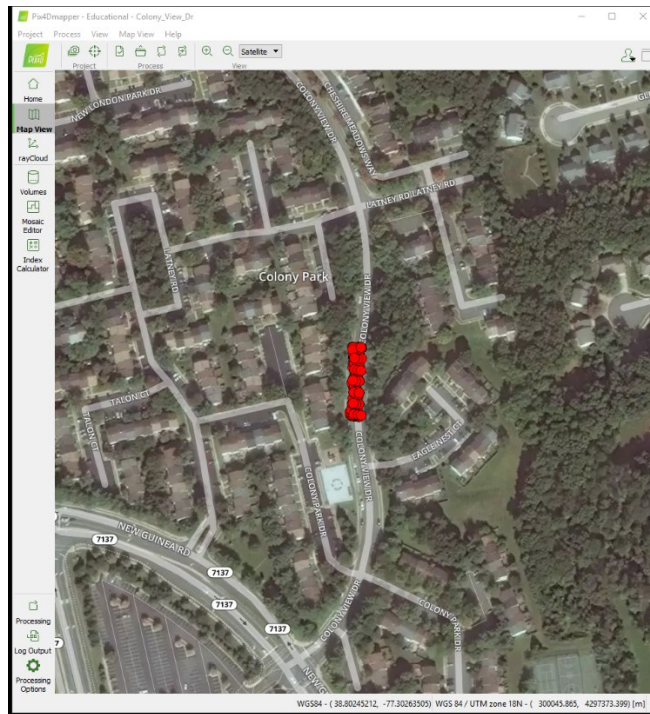


**Figure 45. Pilot Study Site 2: Colony View Drive**

The altitude during the aerial survey was at 25 m to ensure the safety of the drone and the flight mission. Similar to the first pilot study site, this area was surrounded by tall trees that were approximately 20 – 25 m in height. Total of 98 images were captured and the image overlap percentage was 80% and in nadir view. A straight-path pattern was used for this pilot study’s route design. Collected point cloud data, path, and camera setup can be seen in Figure 46.

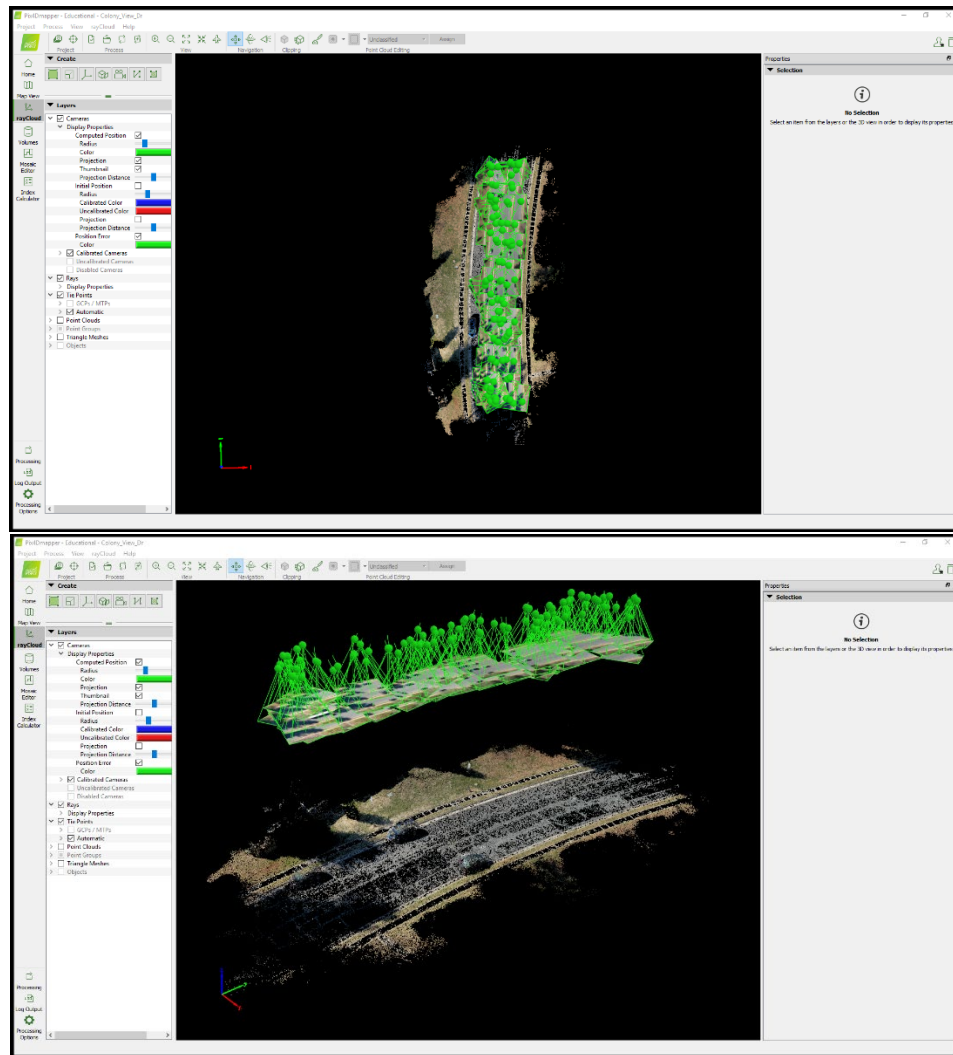


Figure 46. Colony View Drive: Point Cloud and Camera Setup - Top and Side View

At this site, there were four sample potholes that were measured. The collected ground truth data can be found in Table 7 below.

Table 7. Pilot Study 2 Ground Truth Measurement

Sample #	Length	Width	Height
1	15.6 inches	11.5 inches	1.8 inches
2	14.2 inches	11.2 inches	1.6 inches
3	16.2 inches	7.5 inches	1.8 inches
4	17.8 inches	16.9 inches	2.1 inches

In addition, the reference map with the pothole sample number labels can be seen in Figure 47. Colony View Drive: Annotated Potholes. These ground truth data were used to test the accuracy of measurements that were collected using GIS and 3D reconstruction.

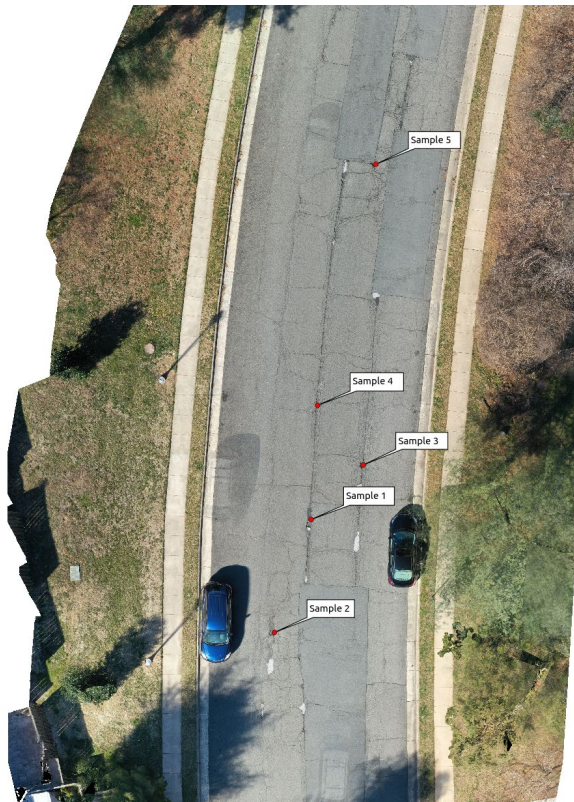


**Figure 47. Colony View Drive: Annotated Potholes**

After the aerial survey was over, these images were then transferred and uploaded to Pix4Dmapper. Based on Pix4Dmapper calculations, the average ground sampling distance was 0.55 cm and 0.5618 acres of land were covered. The median number of keypoints per image was 44,288 keypoints per image. Compared to the first pilot study

site, there were 10,629 more points because this survey area was significantly smaller than the previous pilot study site. All of 98 images were calibrated and the median number of matched keypoints was 22,040 matches per calibrated image. An orthomosaic and the corresponding sparse digital surface model can be seen below.

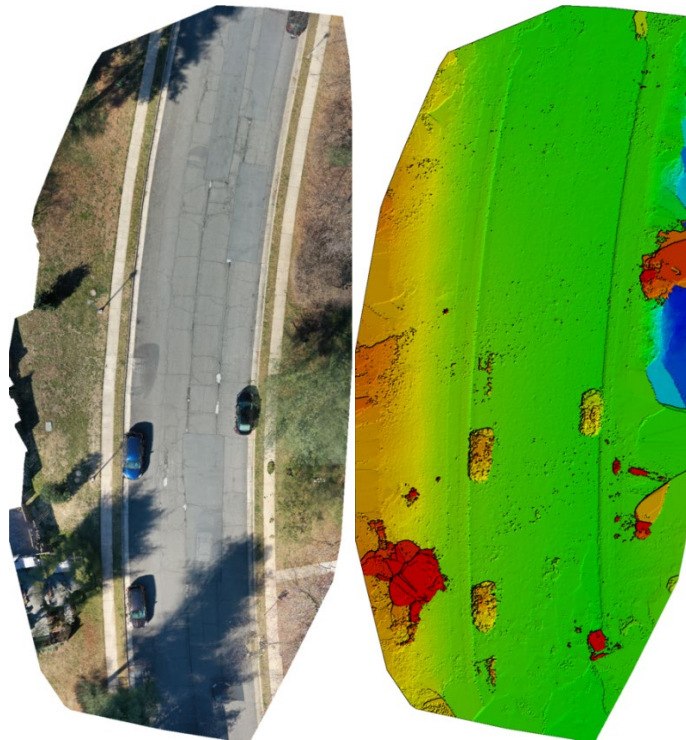


**Figure 48. Colony View Drive: Orthomosaic and DSM**

Time for point cloud densification was approximately 12 minutes 40 seconds, time for point cloud classification was approximately 10 seconds. Time for 3D textured mesh generation was 3 minutes 5 seconds. The number of 3D densified point was 6,976,749 points, 1,155,587 points less than the first pilot study 3D densified points. The average density per cubic meter was 19,014.2 points, and the digital surface model and

orthomosaic resolution was 0.549 cm/pixel. Time for DSM generation was 6 minutes 16 seconds and time for orthomosaic generation was 10 minutes 24 seconds. Overall, the entire data processing time took 32 minutes.

The result of GIS was a file geodatabase that contained an orthomosaic road clipped image, a pothole shapefile with x, y, z coordinates of the potential potholes, length, width, height, and other attributes such as road names, jurisdiction, postal code, and road class. The clipped road image of Colony View Drive and the attribute table of the potholes can be seen in Figure 49.



FID*	Shape*	Join_Count	TARGET_FID	POINT_X	POINT_Y	Class_Type	Length	Width	Height	Join_Count	TARGET_FID	OBJECTID	TYPE	EFFECTIVE	EXPIRY_DAT	SOURCE	PERVI
1	Point	1	1102	-77.300243	38.801312	0	15.8	11.5	0	1	0	2104	Paved Road	2012-10-19T00:00:00.000Z		2009 Stereo Models	
2	Point	1	1102	-77.300268	38.801251	0	13.9	11.8	0	1	1	2104	Paved Road	2012-10-19T00:00:00.000Z		2009 Stereo Models	
3	Point	1	1102	-77.300207	38.801346	0	18.2	7.7	0	1	2	2104	Paved Road	2012-10-19T00:00:00.000Z		2009 Stereo Models	
4	Point	1	1102	-77.300203	38.801614	0	17.3	16.3	0	1	3	2104	Paved Road	2012-10-19T00:00:00.000Z		2009 Stereo Models	

**Figure 49. Colony View Drive: Clipped Road and Pothole Data**

After potential potholes have been manually identified in the GIS, the point cloud was imported into CloudCompare to extract those potholes and surrounding point cloud data. For this pilot study, four potential potholes have been extracted. Point cloud data surrounding these four potholes have been clipped, segmented, and filtered. These four point cloud samples can be seen in Figure 50.

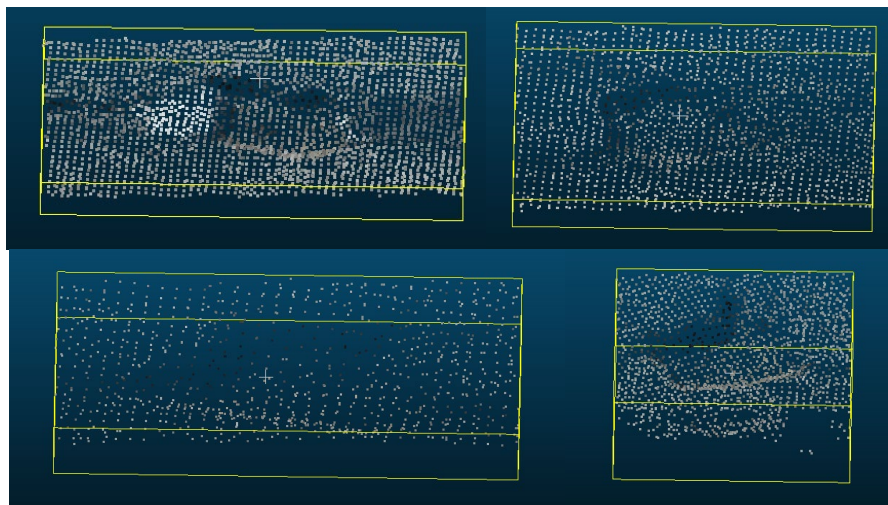


**Figure 50. Colony View Drive: Clipped Point Cloud Samples 1, 2, 3, 4**

The first three samples were not filtered due to low noise. Only Sample 4 was filtered because of high noise and many outliers. Sample 4 side view before and after filter can be seen in Figure 51. Sample 1 contained 2,701 points, Sample 2 contained 1,923 points, Sample 3 contained 1,003 points, and Sample 4 contained 1,789 points (1,360 points after filter). These sample point cloud data were exported as .las file and transferred to Autodesk ReCap Pro for conversion. After the conversion process, the .rcs point cloud files were loaded into Civil 3D for measuring the depth of the potholes using

two TIN surfaces. The TIN surfaces were generated using the boundary, base surface of the point cloud and the TIN surface model of the pothole point cloud.

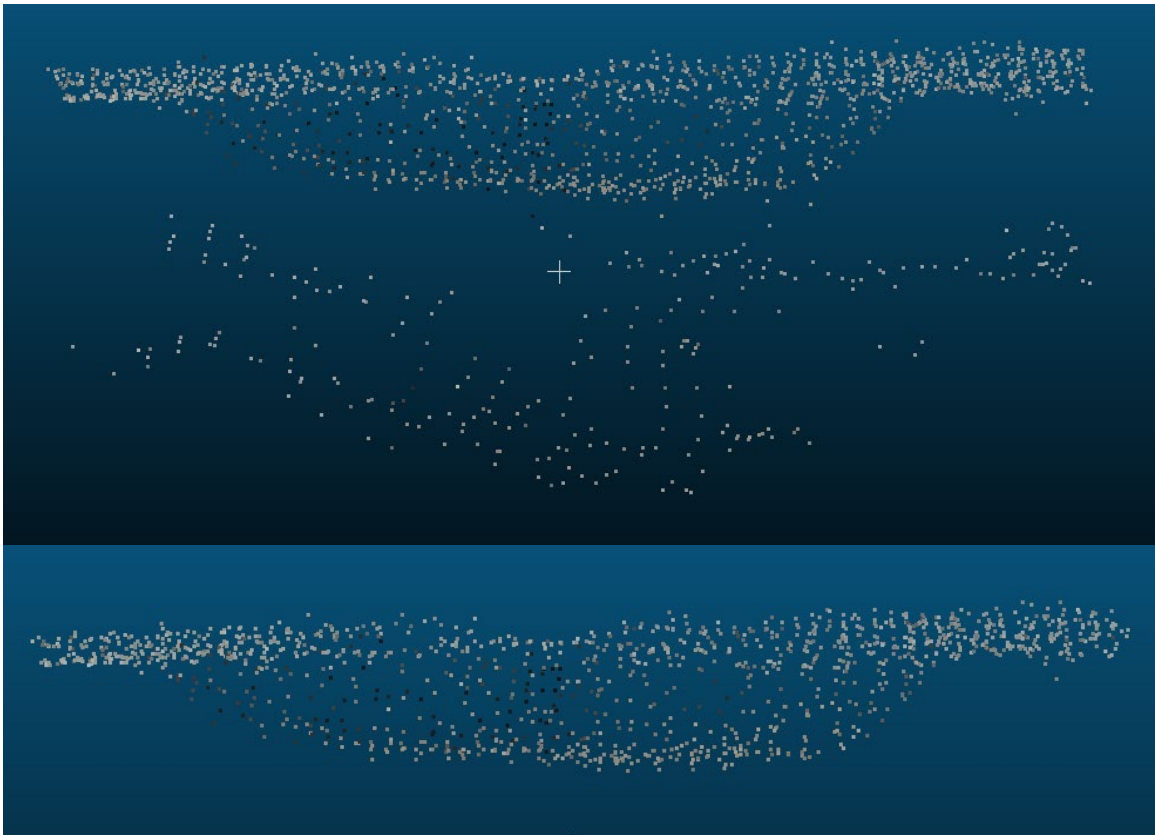


**Figure 51. Colony View Drive: Sample 4 Side View Filtered**

TIN surface was created using the sample 1, 2, 3, 4 point cloud data and Kriging interpolation method. Figure 52 depicts the Sample 1 TIN surface layer.

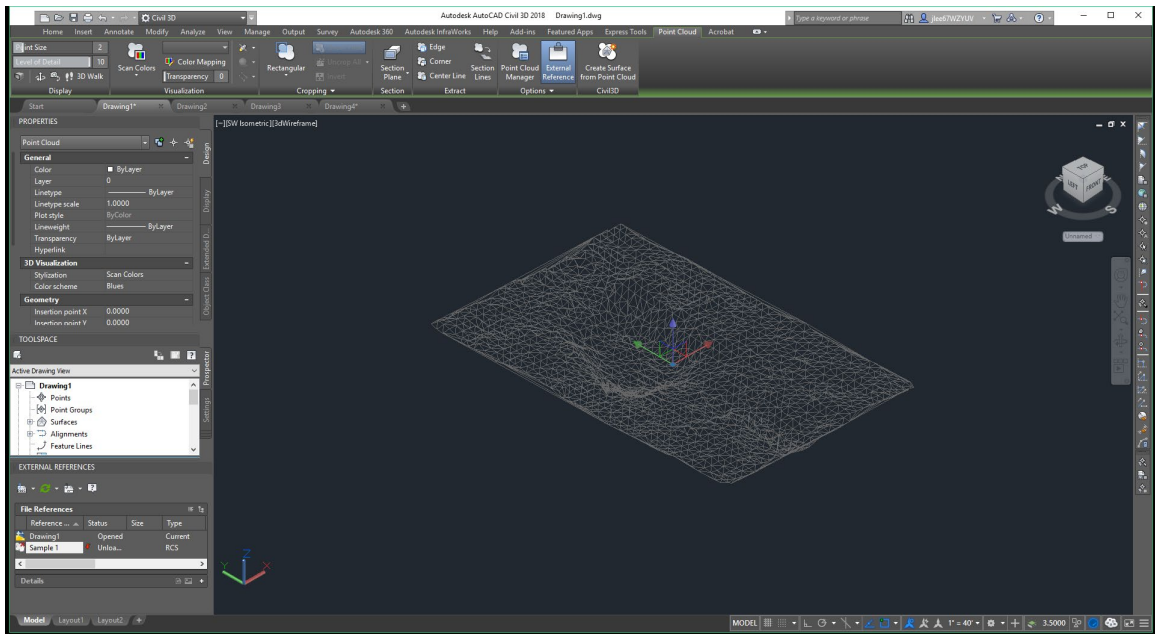
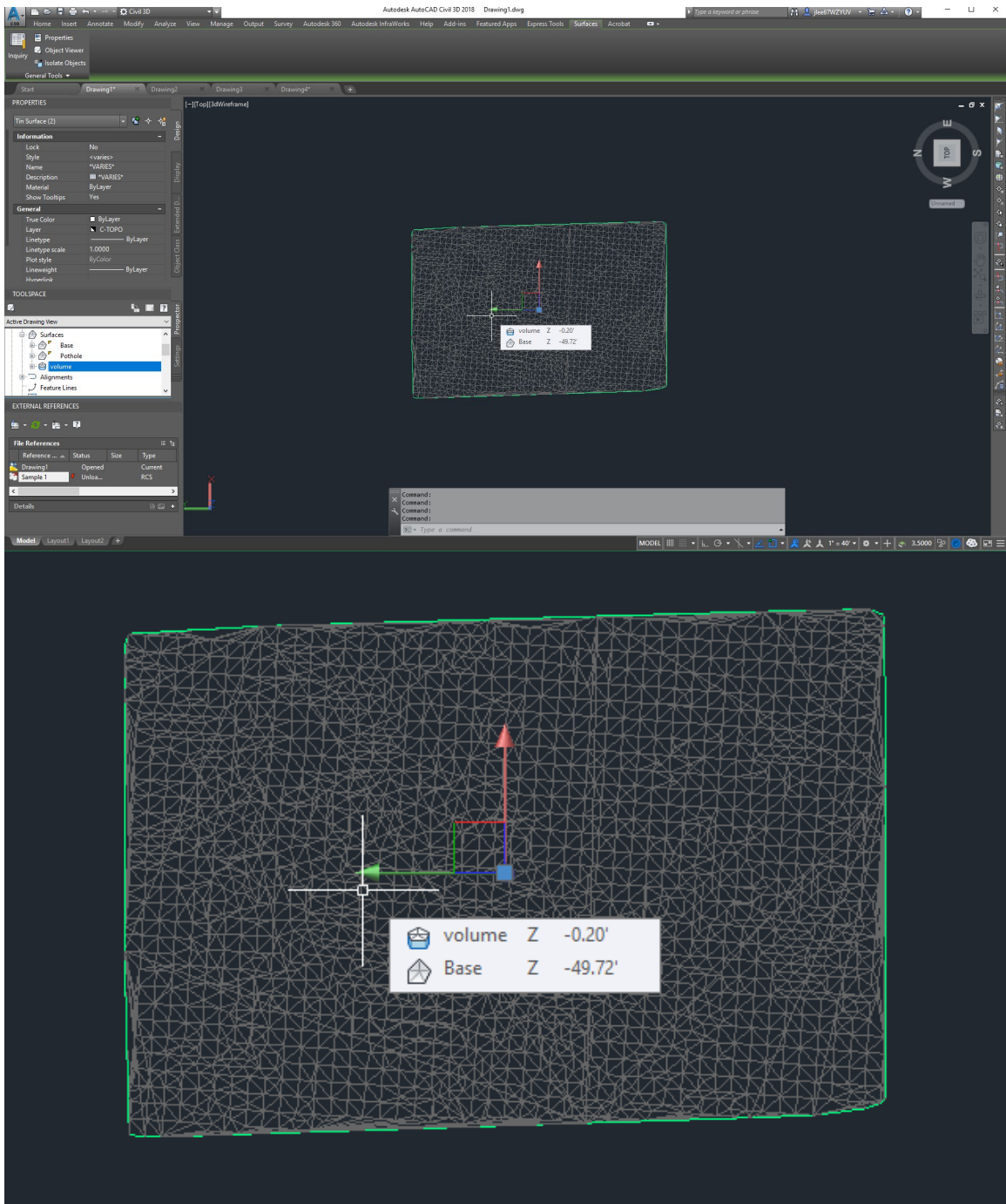


Figure 52. Colony View Drive: Sample 1 Point Cloud in Civil 3D

Following the method as pilot study 1, a surface layers were created using the boundary polyline of the point cloud data. The flat base surface layers were used to subtract z-value from the base to the pothole TIN surface layers. The calculated Z-value for Sample 1 can be seen in Figure 53.



**Figure 53. Colony View Drive: Sample 1 Z-value**

The z-values of each pothole are listed in Table 8 below. After collecting the height information from 3D reconstruction step, Z-value or height value was included in

the Pilot Study 2: Colony View Drive geodatabase. The size accuracy of the potholes was calculated using the ground truth measurement data and the GIS and 3D reconstruction measured data.

**Table 8. Pilot Study 2 Identified Measurement**

<b>Sample #</b>	<b>Length</b>	<b>Width</b>	<b>Height</b>
1	15.8 inches	11.5 inches	2.0 inches
2	13.9 inches	11.8 inches	1.5 inches
3	18.2 inches	7.7 inches	1.6 inches
4	17.3 inches	16.3 inches	2.3 inches

Based on the ground truth measurement data and identified measurement data of Sample 2, absolute accuracy values of the identified measurement are depicted in Table 9.

**Table 9. Pilot Study 2 Identified Measurement Accuracy**

<b>Sample #</b>	<b>Length</b>	<b>Width</b>	<b>Height</b>
1	+0.2 inches	0 inches	+0.2 inches
2	-0.3 inches	+0.6 inches	-0.1 inches
3	+2.0 inches	+0.2 inches	-0.2 inches
4	-0.5 inches	-0.6 inches	+0.2 inches

Length measurement: +0.2 inches, width measurement: 0 inch, and height measurement: +0.2 inches. Sample 2 length measurement: -0.3 inches, width: +0.6 inches, and height: -0.1 inches. Sample 3 length measurement: +2.0 inches, width: +0.2 inches, and height: -0.2 inches. Sample 4 length measurement: -0.5 inches, width: -0.6

inches, and height: +0.2 inches. The results of Pilot Study 2 were promising since the identified measurement value had an absolute accuracy of +/- 2.0 inch.

## CHAPTER FIVE: CONCLUSIONS

The process and applications of this thesis research present exciting opportunities for using widely accessible drone platforms to create 3D geospatial dataset that contains dimension information, severity level, x and y coordinates, and other critical information that will help local transportation authorities with assessing and prioritizing repair areas. The relative ease of using simple UAVs, photogrammetry processing, GIS and 3D modeling software suggest the thesis pipeline as a viable method for obtaining pothole information from aerial images. Reviewing the current literature and research journals reveals that the 2D vision-based and 3D reconstruction-based workflow is a highly desired method, and is pursued within the fields of computer vision, topographic survey, infrastructure inspection, and environmental monitoring. Utilizing this thesis workflow can greatly contribute to research applications searching for accessible, accurate, and straight-forward methods for collecting aerial images for road inspections, generating 3D geospatial dataset containing critical information, and detecting potential potholes from imagery, especially from consumer grade aerial platforms. Three main methods were developed that provide solutions to identifying, measuring, validating, and identifying potholes from aerial images. Pilot studies were conducted at different test sites and these experiments helped examine what environmental factors had significant impacts on the quality of output results. Different flight settings were tested. Based on the surrounding

environmental conditions from different pilot study sites, the best altitude for aerial surveying of the roads was found to be at 20-25 m. During aerial surveying, there are features that present difficulties for aerial imagery capture, photogrammetric processing, and 3D modeling. For aerial imagery capture step, it is necessary to use the optimal flight environment settings for collecting high quality aerial image data which will be used in the photogrammetric processing step. During photogrammetric processing step, it is important to tweak and use different setting combinations such as limiting the number of keypoint matches and points in the point cloud data. Due to texturing and surface modeling, 3D modeling process requires very high-quality point cloud data. Before reconstructing 3D models, it is necessary to filter and remove noise on the point cloud data to obtain accurate 3D pothole models. Software used in this project (Pix4D, Autodesk Civil 3D, ReCap Pro, ESRI ArcMap 10.6.1, MATLAB, CloudCompare) were chosen due to their broad, long-term support and reliability. Although the primary software used were commercial software, many other open source software can be used to replicate the process and achieve similar results.

### **5.1 Future Research**

The method and workflow executed in this research proved a working demonstration of creating 3D geospatial data from aerial imagery using photogrammetric, mapping, and 3D modeling processes. Future research regarding this thesis project will focus around using more open source software, replicating the steps, and producing similar results. In addition, alternative equipment and options can be researched to improve the overall pothole identification method.

## REFERENCES

- [1] “Beyond Traffic Framework 2045: Trends and Choices.” U.S. Department of Transportation.
- [2] L. M. Pierce, G. McGovern, and K. A. Zimmerman, “Practical Guide for Quality Management of Pavement Condition Data Collection,” U.S. Department of Transportation Federal Highway Administration, Feb. 2013.
- [3] K. A. Zimmerman, *Pavement Management Methodologies to Select Projects and Recommend Preservation Treatments*. Washington, D.C: Transportation Research Board, 1995.
- [4] “The Long-Term Pavement Performance Program,” Federal Highway Administration - Office of Research, Development, and Technology: Infrastructure R&D, Turner-Fairbank Highway Research Center, 6300 Georgetown Pike, McLean, VA 22101, FHWA-HRT-15-049, Sep. 2015.
- [5] D. E. Peterson, *Pavement Management Practices*. Washington, D.C: Transportation Research Board, National Research Council, 1987.
- [6] S. S. Adlinge and A. K. Gupta, “Pavement Deterioration and its Causes,” p. 7.
- [7] J. S. Miller and W. Y. Bellinger, “Distress Identification Manual for the Long-Term Pavement Performance Program,” Federal Highway Administration - Office of Research, Development, and Technology: Infrastructure R&D, Turner-Fairbank Highway Research Center, 6300 Georgetown Pike, McLean, VA 22101, Technical Report FHWA-RD-03-031, Jun. 2003.
- [8] A. Akagic, E. Buza, and S. Omanovic, “Pothole detection: An efficient vision based method using RGB color space image segmentation,” in *2017 40th International Convention on Information and Communication Technology, Electronics and Microelectronics (MIPRO)*, 2017, pp. 1104–1109.
- [9] T. Kim and S.-K. Ryu, “Review and Analysis of Pothole Detection Methods,” 2014. [Online]. Available: /paper/Review-and-Analysis-of-Pothole-Detection-Methods-Kim-Ryu/41d8189111cc320a2fd8444b0bf13a6263f45807. [Accessed: 14-Aug-2018].
- [10] Y. O. Ouma and M. Hahn, “Pothole detection on asphalt pavements from 2D-colour pothole images using fuzzy c-means clustering and morphological reconstruction,” *Automation in Construction*, vol. 83, pp. 196–211, Nov. 2017.
- [11] Yu Bill X. and Yu Xinbao, “Vibration-Based System for Pavement Condition Evaluation,” *Applications of Advanced Technology in Transportation (2006)*.
- [12] K. De Zoysa, C. Keppitiyagama, G. P. Seneviratne, and W. W. A. T. Shihan, “A public transport system based sensor network for road surface condition monitoring,”

- in *Proceedings of the 2007 workshop on Networked systems for developing regions - NSDR '07*, Kyoto, Japan, 2007, p. 1.
- [13] J. Eriksson, L. Girod, B. Hull, R. Newton, S. Madden, and H. Balakrishnan, "The pothole patrol: using a mobile sensor network for road surface monitoring," in *Proceeding of the 6th international conference on Mobile systems, applications, and services - MobiSys '08*, Breckenridge, CO, USA, 2008, p. 29.
- [14] D. Zhang *et al.*, "Automatic pavement defect detection using 3D laser profiling technology," *Automation in Construction*, vol. 96, pp. 350–365, Dec. 2018.
- [15] Hou Zhiqiong, Wang Kelvin C. P., and Gong Weiguo, "Experimentation of 3D Pavement Imaging through Stereovision," *International Conference on Transportation Engineering 2007*.
- [16] R. Fan, X. Ai, and N. Dahnoun, "Road surface 3d reconstruction based on dense subpixel disparity map estimation," *IEEE Transactions on Image Processing*, vol. 27, no. 6, pp. 3025–3035, Jun. 2018.
- [17] S. S. Rode, S. Vijay, P. Goyal, P. Kulkarni, and K. Arya, "Pothole Detection and Warning System: Infrastructure Support and System Design," in *2009 International Conference on Electronic Computer Technology*, 2009, pp. 286–290.
- [18] P. Wang, Y. Hu, Y. Dai, and M. Tian, "Asphalt Pavement Pothole Detection and Segmentation Based on Wavelet Energy Field," *Mathematical Problems in Engineering*, vol. 2017, pp. 1–13, 2017.
- [19] S.-K. Ryu, T. Kim, and Y.-R. Kim, "Feature-Based Pothole Detection in Two-Dimensional Images," *Transportation Research Record*, no. 2528, pp. 9–17, 2015.
- [20] Radopoulou Stefania C., Brilakis Ioannis, Doycheva Kristina, and Koch Christian, "A Framework for Automated Pavement Condition Monitoring," *Construction Research Congress 2016*.
- [21] K. A. Zimmerman, National Cooperative Highway Research Program, National Cooperative Highway Research Program Synthesis Program, Synthesis Program, Transportation Research Board, and National Academies of Sciences, Engineering, and Medicine, *Pavement Management Systems: Putting Data to Work*. Washington, D.C.: Transportation Research Board, 2017.
- [22] "Pavement Management Visual Distress Survey Manual." South Dakota Department of Transportation, 11-May-2017.
- [23] A. Mednis, G. Strazdins, R. Zviedris, G. Kanonirs, and L. Selavo, "Real time pothole detection using Android smartphones with accelerometers," in *2011 International Conference on Distributed Computing in Sensor Systems and Workshops (DCOSS)*, 2011, pp. 1–6.
- [24] L. Ying and E. Salari, "Beamlet Transform-Based Technique for Pavement Crack Detection and Classification," *Computer-Aided Civil and Infrastructure Engineering*, vol. 25, no. 8, pp. 572–580, Nov. 2010.
- [25] Y. O. Ouma and M. Hahn, "Pothole detection on asphalt pavements from 2D-colour pothole images using fuzzy c -means clustering and morphological reconstruction," *Automation in Construction*, vol. 83, pp. 196–211, Nov. 2017.

- [26] J. Lin and Y. Liu, "Potholes Detection Based on SVM in the Pavement Distress Image," in *2010 Ninth International Symposium on Distributed Computing and Applications to Business, Engineering and Science*, 2010, pp. 544–547.
- [27] "Pothole detection in asphalt pavement images," *Advanced Engineering Informatics*, vol. 25, no. 3, pp. 507–515, Aug. 2011.
- [28] L. Huidrom, L. K. Das, and S. K. Sud, "Method for Automated Assessment of Potholes, Cracks and Patches from Road Surface Video Clips," *Procedia - Social and Behavioral Sciences*, vol. 104, pp. 312–321, Dec. 2013.
- [29] Y. Jo and S. Ryu, "Pothole Detection Using Android Smartphone with a video camera," vol. 8, no. 1, p. 5, 2017.
- [30] R. Fan, Y. Liu, X. Yang, M. J. Bocus, N. Dahnoun, and S. Tancock, "Real-Time Stereo Vision for Road Surface 3-D Reconstruction," *arXiv:1807.07433 [cs]*, Jul. 2018.
- [31] M. Staniek, "Neural Networks in Stereo Vision Evaluation of Road Pavement Condition," p. 8, 2015.
- [32] Q. Li, M. Yao, X. Yao, and B. Xu, "A real-time 3D scanning system for pavement distortion inspection," *Meas. Sci. Technol.*, vol. 21, no. 1, p. 015702, 2010.
- [33] Chang K. T., Chang J. R., and Liu J. K., "Detection of Pavement Distresses Using 3D Laser Scanning Technology," *Computing in Civil Engineering (2005)*.
- [34] I. Moazzam, K. Kamal, S. Mathavan, S. Usman, and M. Rahman, "Metrology and visualization of potholes using the microsoft kinect sensor," in *16th International IEEE Conference on Intelligent Transportation Systems (ITSC 2013)*, 2013, pp. 1284–1291.
- [35] D. Joubert, A. Tyatyantsi, J. Mphahlehle, and V. Manchidi, "Pothole tagging system," Nov. 2011.
- [36] N. Pfeifer, P. Glira, and C. Briese, "DIRECT GEOREFERENCING WITH ON BOARD NAVIGATION COMPONENTS OF LIGHT WEIGHT UAV PLATFORMS," *ISPRS - International Archives of the Photogrammetry, Remote Sensing and Spatial Information Sciences*, vol. XXXIX-B7, pp. 487–492, Aug. 2012.
- [37] S. O'Donnell, "A Short History of Unmanned Aerial Vehicles," *Consortiq*, 16-Jun-2017. [Online]. Available: <https://consortiq.com/media-centre/blog/short-history-unmanned-aerial-vehicles-uavs>. [Accessed: 19-Feb-2019].
- [38] B. Custers, Ed., *The Future of Drone Use: Opportunities and Threats from Ethical and Legal Perspectives*, vol. 27. The Hauge, Netherlands: T.M.C. Asser Press, 2016.
- [39] I. Colomina and P. Molina, "Unmanned aerial systems for photogrammetry and remote sensing: A review," *ISPRS Journal of Photogrammetry and Remote Sensing*, vol. 92, pp. 79–97, Jun. 2014.
- [40] M. A. Boon, R. Greenfield, and S. Tesfamichael, "Unmanned Aerial Vehicle (UAV) photogrammetry produces accurate high-resolution orthophotos, point clouds and surface models for mapping wetlands," *South African Journal of Geomatics*, vol. 5, no. 2, p. 186, Sep. 2016.

- [41] J. R. K. Lehmann *et al.*, “Open-Source Processing and Analysis of Aerial Imagery Acquired with a Low-Cost Unmanned Aerial System to Support Invasive Plant Management,” *Frontiers in Environmental Science*, vol. 5, Jul. 2017.
- [42] F. Remondino, L. Barazzetti, F. Nex, M. Scaioni, and D. Sarazzi, “UAV PHOTOGRAMMETRY FOR MAPPING AND 3D MODELING – CURRENT STATUS AND FUTURE PERSPECTIVES,” *ISPRS - International Archives of the Photogrammetry, Remote Sensing and Spatial Information Sciences*, vol. XXXVIII-1/C22, pp. 25–31, Sep. 2012.
- [43] H. Zakeri, F. M. Nejad, and A. Fahimifar, “Image Based Techniques for Crack Detection, Classification and Quantification in Asphalt Pavement: A Review,” *Arch Computat Methods Eng*, vol. 24, no. 4, pp. 935–977, Nov. 2017.
- [44] S. Cafiso, A. D. Graziano, and S. Battiato, “Evaluation Of Pavement Surface Distress Using Digital Image Collection And Analysis,” p. 10.
- [45] M. P. Christiansen, M. S. Laursen, R. N. Jørgensen, S. Skovsen, and R. Gislum, “Designing and Testing a UAV Mapping System for Agricultural Field Surveying,” *Sensors*, vol. 17, no. 12, p. 2703, Dec. 2017.
- [46] E. Schnebele, B. F. Tanyu, G. Cervone, and N. Waters, “Review of remote sensing methodologies for pavement management and assessment,” *Eur. Transp. Res. Rev.*, vol. 7, no. 2, p. 7, Mar. 2015.
- [47] Zhang Su and Bogus Susan M., “Use of Low-cost Remote Sensing for Infrastructure Management,” *Construction Research Congress 2014*.
- [48] C. Mettas, K. Themistocleous, K. Neocleous, A. Christofe, K. Pilakoutas, and D. Hadjimitsis, “Monitoring asphalt pavement damages using remote sensing techniques,” presented at the Third International Conference on Remote Sensing and Geoinformation of the Environment, Paphos, Cyprus, 2015, p. 95350S.
- [49] M. I. Sameen, B. Pradhan, and O. S. Aziz, “Classification of Very High Resolution Aerial Photos Using Spectral-Spatial Convolutional Neural Networks,” *Journal of Sensors*, 2018. [Online]. Available: <https://www.hindawi.com/journals/js/2018/7195432/>. [Accessed: 02-Dec-2018].
- [50] Y. Pan, X. Zhang, G. Cervone, and L. Yang, “Detection of Asphalt Pavement Potholes and Cracks Based on the Unmanned Aerial Vehicle Multispectral Imagery,” *IEEE Journal of Selected Topics in Applied Earth Observations and Remote Sensing*, vol. 11, no. 10, pp. 3701–3712, Oct. 2018.
- [51] J. Choi, L. Zhu, and H. Kurosu, “DETECTION OF CRACKS IN PAVED ROAD SURFACE USING LASER SCAN IMAGE DATA,” *ISPRS - International Archives of the Photogrammetry, Remote Sensing and Spatial Information Sciences*, vol. XLI-B1, pp. 559–562, Jun. 2016.
- [52] W. Uddin, “Evaluation of Airborne LIDAR Digital Terrain Mapping for Highway Corridor Planning and Design,” *Conference Proceedings*, p. 7, 2002.
- [53] H. M. Jol, *Ground Penetrating Radar Theory and Applications*. Elsevier, 2008.
- [54] M. Rumpler *et al.*, “Automated End-to-End Workflow for Precise and Geo-accurate Reconstructions using Fiducial Markers,” *ISPRS Annals of Photogrammetry, Remote Sensing and Spatial Information Sciences*, vol. II-3, pp. 135–142, Aug. 2014.

## **BIOGRAPHY**

Jin Kyu Lee graduated from Battlefield High School, Haymarket, Virginia, in 2011. He received his Bachelor of Science in Criminology, Law and Society from George Mason University in 2016. He was employed as a Research Assistant by the National Consortium for the Study of Terrorism and Responses to Terrorism research center at University of Maryland, College Park for counterterrorism-related projects. During his first two years of graduate program career, he worked on a federal-government funded project on unmanned logistics systems for the Office of Naval Research, Code 30 Program. In his last year of graduate program, he was a Graduate Teaching Assistant for four undergraduate courses in the Department of Geography and Geoinformation Science at George Mason University. He earned his Master of Science in Geoinformatics and Geospatial Intelligence from George Mason University in 2019.